JUMR

Journal of Undergraduate Materials Research

Alfred Knobler Inaugural Issue

Letter from the Editorial Board

Hello Friends,

We are pleased to present to you the Alfred E. Knobler inaugural issue of the *Journal of Undergraduate Materials Research* (JUMR), a journal dedicated to undergraduates working in the field of Materials Science and Engineering. This is a proud moment for the Virginia Tech Department of Materials Science and Engineering (MSE), and we congratulate the selected authors.

The idea for this journal originated from discussions regarding the lack of a platform highlighting undergraduate research. We hope that this annual publication will provide a venue for undergraduates to showcase their research, improve their technical writing skills, and be exposed to the rigors of peer-reviewed publishing.

During the development of the concept, the benefits of collaborating with the Department of English became apparent. This joint effort was realized as a service project of ENGL 3824, "Designing Documents for Print," and is representative of the goals of Alfred E. Knobler, an alumnus of MSE and a strong supporter of both departments, to whom we dedicate this inaugural issue.

Again, we would like to thank the students who contributed articles to make this project a success. We cannot overstate the assistance of the students, faculty, and staff of MSE at Virginia Tech. Special thanks is also due to David Clark and Diane Folz for inspiring this project.

We hope that this periodical will be a strong voice of the research achievements of undergraduates in the field of MSE.

Editorial Board

On the cover:
Pieces of the Pilgrim Glass collection permanently displayed in Holden Hall.

This collection was donated to MSE by Alfred Knobler in 1998. The collection includes several pieces of cameo glass as well as cranberry, cobalt, and other glasswares for which Pilgrim Glass became internationally recognized during its 50-plus year history.

Materials Science and Engineering
discover what we're made of...

Cover photo by:
Elizabeth Jeffers, Adam Maisano, and Ben Poquette

Contents

Features

Alfred Knobler pg. 8

Research

Scanning Electron Micrograph
of Powder EOS™ PA pg. 17

Featured Department

Microstructure of YBCO
pg. 36 (D)

Editorial Credits

Disclaimer

The views, opinions and findings contained in the enclosed works are those of the individual authors. The publisher, editors, and authors assume neither responsibility nor liability for errors or any consequences arising from the use of the information contained herein. Mention of trade names or commercial products does not constitute endorsement or recommendations for use by the publishers, editors, or authors.

Final determination of the suitability of any information, procedure, or product for use contemplated by any user, and the manner of that use, is the sole responsibility of the user. This collection of works is intended for informational purposes only. Expert advice should be obtained at all times when implementation is being considered, particularly where hazardous materials or processes are encountered.

Virginia Tech:
The Place for Materials Education and Research

by David Clark, Professor and Department Head

These are exciting times for the Department of Materials Science and Engineering (MSE). In August 2004, we hired five faculty members with a range of expertise including ceramics, photonics, and nanomaterials. Our existing faculty and staff have worked hard to prepare space and provide resources for the new faculty. Two of the new members, Levon Asryan and Yu Wang, are heavily involved in computational materials science and will take advantage of Virginia Tech's supercomputer, System X, which is ranked among the fastest in the world. They will

---

Within five years, we expect the AMCF to house approximately \$12M in research equipment.

---

join Professor Diana Farkas, already a renowned researcher in the area of simulation of fracture and diffusion, and others within the engineering and science faculty in a "computational materials science cluster." In addition to broadening the department's research directions, these faculty will strengthen the computational components of the graduate and undergraduate curricula. Gary Pickrell and Kathy Lu are experimentalists and will apply their expertise in ceramics and nanomaterials to the development of sensors, fuel cells and photonic devices. Kathryn Logan, hired as the NASA Langley Professor, will coordinate research and education activities between Virginia Tech and the new National Institute of Aerospace (NIA). Professor Logan is a past president of the American Ceramic Society and the National Institute of Ceramic Engineers. She is also a Fellow in both of these professional organizations. It is a rare opportunity for an MSE department to be able to hire five new tenure-track faculty in one season,

and we are grateful for the confidence and support provided by the College of Engineering. These new hires move us a large step forward toward our goal of 19 full-time faculty.

MSE is playing a major role in the new Institute for Critical Technology and Applied Science (ICTAS). The Institute (pg. 7) will provide infrastructure and space to further synergistic research between engineering and the sciences. When fully operational, ICTAS will occupy several buildings, one of which will be located behind Holden Hall, the present home of MSE. Nanotechnology and Advanced Materials are among the focus areas for the Institute. Under the leadership of Professors Carlos Suchicital and Bill Reynolds, MSE has designed an advanced materials Characterization Facility (AMCF) that will occupy about $15,000$ ft^2 in a new building at the Corporate Research Center (CRC). The University has already provided \$3.2M to purchase a state-of-the-art TEM and an ion microprobe. Within five years, we expect the AMCF to house approximately \$12M in research equipment. In addition to pulling together the diverse materials community across the university, ICTAS will attract top-notch faculty and graduate students to Virginia Tech.

Each fall, MSE hosts an open house for freshmen as they attempt to select a home department. This year, over 400 students attended a well-organized program consisting of demonstrations, information sessions, and refreshments. Through recruiting events such as this, we expect to reach our goal of about 100 undergraduate students. The department is grateful to Alex Aning, Chair of the Recruiting Committee, Jan Doran, the Undergraduate Program Services Coordinator, and the student-run Materials

---

Our goal is 95 graduate students, producing about 15-20 Ph.D. degrees per year.

Engineering Professional Societies (MEPS) for organizing and running this event.

At its September 2004 meeting, the MSE Advisory Board considered a variety of new initiatives, provided input towards the continuing improvement of program quality, and discussed ways to promote the growth of the graduate program. In the latter regard, our goal is a program with approximately 95 graduate students, producing about 15-20 Ph.D. degrees per year. A major obstacle in achieving this goal is shrinking federal and state government support of basic research. In the future, we will have to rely more on industrial support, fellowships, endowments, and fund-raising activities. Thus it is appropriate that this first issue of the *Journal of Undergraduate Materials Research* is dedicated to Alf Knobler, an alumnus who has donated substantial funds to Virginia Tech.

Alf was one of the first to bridge engineering principles with artistic design.

Alf graduated with a Bachelor of Science in Ceramic Engineering (now part of the Department of Materials Science and Engineering) from Virginia Tech in 1938. He purchased Tri-State Glass Manufacturing Company, located in Huntington, West Virginia, in 1949, which became Pilgrim Glass. In 1956, he moved the facility to Ceredo, West Virginia. A wide array of artistic glasses (e.g. cameos and cranberry) were manufactured for over 50 years (see cover). Alf was one of the first to bridge engineering principles with artistic design. In addition to being a visionary in ceramics and glasses, he has a wide range of interests in literature, poetry, history, politics, and diversity. He recently established the Knobler Scholars Program (pg. 9) to support graduate students in the Departments of English and Materials Science and Engineering. In addition to providing financial support to students from both departments, this program has several cooperative projects such as this student journal and the annual Knobler Summits, which feature a world renowned lecturer. This cooperation has also strengthened an already strong communications program in MSE. Indeed, this program represents the true spirit of a university!

David Clark
Professor and Head
Dept. of MSE
Virginia Tech

Molten stainless steel is poured into the top of an investment casting. Students watched this as part of a foundry tour hosted by Conbraco.
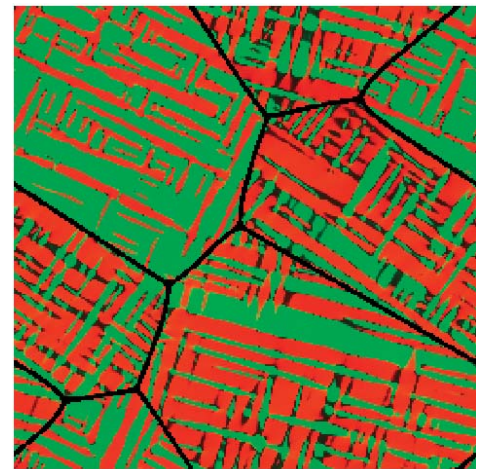
A 2-dimensional phase-field computer simulation, by Todd Heil, of the martensitic microstructure in a polycrystalline Fe – 31at% Ni alloy. Red and green regions possess the same martensitic crystal structure, but have different orientations.

David Clark with a group of MSE students at the American Ceramic Society annual conference in Baltimore, MD, Spring 2005.

MSE on the Move

by Carlos Suchicital, Research Associate Professor

Planned Institute for Critical Technology and Applied Science Building

The new Institute for Critical Technology and Applied Science (ICTAS) will attract top faculty and students, foster collaboration between researchers, increase research funding, and provide infrastructure and space to facilitate these aims. The ICTAS Initiative at Virginia Tech (led by the College of Engineering) will involve the construction of several new buildings comprising a multi-disciplinary research laboratory and a 15,000 ft^2 state-of-the-art Advanced Materials Characterization Facility (AMCF). The AMCF facility will be formed by a collection of new and existing tools for processing, characterizing, and testing materials at the macro, micro, and nanometer scales. Of the expected cost of $12M in equipment for the AMCF, the University has already provided $3.2M to purchase a High-Resolution Transmission Electron Microscope (HRTEM) and an ion microprobe. The equipment to be housed in the AMCF includes:

- Electron Microscopes
  - Scanning Electron Microscope
  - HRTEM
  - Environmental Scanning Electron Microscope
- Secondary Ion Mass Spectroscope
- Nano-Indenter, Nano-Structure Manipulator, and Nano-Lithography Systems
- Ferromagnetic/Ferroelectric Properties Measurement Systems
- Ion Miller
- Focused Ion Beam
- Optical Microscopes
- Atomic Force Microscopes
  - Nano-Manipulation Capabilities
- X-ray Diffractometers
- X-ray Tomograph
- X-ray Photoelectron Spectrometer
- Zeta Potentiometer
- Clean Room Facility
  - Plasma Etching, Film Deposition
  - Mask Aligners, Film Thickness Tester
  - Wet Benches, Spin Casters
  - Annealing/Doping Furnaces

- Thermal Analysis
  - Differential Thermal Analyzer
  - Differential Scanning Calorimeter
  - Thermogravimetric Analyzer
  - Dynamic Mechanical Analysis Dilatometer
- Plasma Spray
- Spectrometer
  - Ultraviolet-Visible-Near Infrared
  - Fourier Transform Infrared
- Dielectric Properties Measurement System
- Nuclear Magnetic Resonance
- Ellipsometer
- Particle Size Analyzer
- Surface Area/Pore Analyzer
- Laser Ablation System
- Cryo-Mill
- Fluid Energy Mill
- Rapid Prototyping Instrument
- Metallorganic Chemical Vapor Deposition Facility
  - MOCVD Hot Wall Reactor
  - Wet Benches
  - Sample Testing

Meet Alfred Knobler

by Susan Holt, Graduate Student

Alfred E. Knobler made several generous donations to Virginia Tech for the creation of Knobler scholarships and fellowships. These opportunities are for both undergraduate and graduate students in the Departments of Materials Science and Engineering and English. The purpose of these scholarships is to foster communication and exchange of ideas and skills between these two departments.

Alfred Knobler was born in the Bronx, New York City, in 1915. His mother emigrated from Hungary in 1888, and his father emigrated from Poland in 1882. When Mr. Knobler was five, his father lost his job. During the Depression, Mr. Knobler saw men and women on the street corners selling apples. Mr.

> ## The purpose of these scholarships is to foster communication and the exchange of ideas...

Knobler stated, "As we made our way into the 1930s, for poor people, and for most people, desperation was the grim reality." However, he and his family persevered, and in 1934, Mr. Knobler entered Virginia Tech, then called Virginia Polytechnic Institute (VPI). At this time, Julian A. Burruss was the university president, Earle Norris was the dean of engineering, and John Whittemore was the head of the Department of Ceramic Engineering.

An important event which would significantly influence Mr. Knobler occurred between 1920 and 1927. Two Italian immigrants, Nicola Sacco and Bartolomeo Vanzetti, were arrested in 1920 on the charge of two counts of murder. Nicolo Sacco was a shoe worker around Boston, and Bartolomeo Vanzetti was a restaurant worker and laborer, and when he settled in Plymouth, Massachusetts, he eventually became a fish peddler. These two men were both radical idealists active in labor struggles. When they were arrested in 1920, there was public outcry that the two were being persecuted because of their outspoken labor ideals. For 7 years, there were trials, appeals, petitions, examinations, and mass meetings. On August 1927, Sacco and Vanzetti were executed. Today, practically

Alfred E. Knobler

no one who studies their case believes that they were guilty.

The effect of the Sacco and Vanzetti case on Mr. Knobler was that he became very active in trying to protect an individual's right to free speech. In a letter to VPI professors who had signed a statement supporting the House Committee on Un-American Activities (1961), Mr. Knobler stated that "Teachers should be in the front line of those demanding 'freedom to think' lest they turn out rubber stamps instead of inquiring students living in an atmosphere which permits democratic dissent."

Mr. Knobler graduated from Virginia Tech in 1938 with a bachelor's degree in Ceramic Engineering. This was at the time of the Depression, so jobs were scarce. Mr. Knobler hitchhiked from the Bronx to Tennessee because he had heard of a porcelain factory in Chattanooga. On the way back, he was picked up by a driver who gave him some insightful advice. The driver told him, "You oughtta sell something. You talk good."

> ## "Teachers should be in the front line of those demanding 'freedom to think'..."

Mr. Knobler took this advice to heart, and when he arrived home, he wrote 75 letters to different ceramic and glass factories in New Jersey. He eventually landed a job with Trenton Potteries, working on

commission. His salary was $35 a week, which was unheard of when the normal weekly income was $10-$12 a week.

During World War II, Mr. Knobler was employed by the War Department as an engineer inspecting steatite, an insulating material produced by war plants. In 1946, at the war's end, Mr. Knobler established Alfred E. Knobler & Co., a national sales organiza-

The thousands of cameo glass blanks...will be brought to life...

tion. In 1949, Mr. Knobler purchased Tri-State Glass Company, a hand-made glass factory operating out of an abandoned garage in Huntington, West Virginia. Before the sale could be completed, Mr. Knobler had to arrange for the factory to receive gas. At that time, there was no pipeline from the Columbia Gas source. Mr. Knobler convinced the gas company to lay the pipe, and the Pilgrim Glass Corporation was born.

The Pilgrim Glass Corporation did not use machines to make replicated glass pieces, but instead used time-honored techniques for making individual glass pieces. Some of these techniques date back to the time of the Romans when glass blowing was first discovered as a viable technique. Some of the intricate pieces produced by Pilgrim Glass include hand-blown crackle glass, glass animals, cranberry glass, and cameo glass. Some consider cameo glass an engineering marvel. Several layers of glass are applied, one on top of another. If the thermal expansion character of each layer is not carefully controlled, then the piece will crack. Once the layers are applied, the top layers are sandblasted by hand so that a specific design shows with the layers being revealed in the design (as shown on the opposite page).

The Pilgrim Glass Corporation closed its doors forever in March 2002. However, Mr. Knobler worked with Margaret Mary Layne, the executive director at the Huntington Museum of Art, to develop the Legacy Cameo Glass Project, which allows some of the artists from Pilgrim Glass to continue their work. The thousands of cameo glass blanks already created at Pilgrim Glass Corporation will be brought to life by artisans at the Huntington Museum of Art.

Mr. Knobler continues to visit Virginia Tech at least once a year. During these visits, he speaks with students about current issues and life in general. During a commencement speech to Department of English students in May 1989, Mr. Knobler related this inspirational poem written over 400 years ago by John Donne which he had read during his English classes at Tech:

"No man is an island, entire of itself;
Everyman is a piece of the continent,
a part of the main.
Any man's death diminishes me,
because I am involved with mankind.
And therefore, never send to know for
whom the bell tolls.
It tolls for thee."

Alfred Knobler with MSE students on a visit to MSE.

Knobler Scholarship Recipients (2004-2005)

Undergraduate Scholarships

Nicholas C. Bell
Vincent P. Caluori
Brian T. Costello
Diane M. Fields
Matthew L. Hubbard
Michael P. Hunt
Matthew E. Lynch
Jennifer E. Mueller
Kristine R. Obusek
Edward R. Parker
Kristin M. Patterson

Alexander W. Scott
Ashley A. White
Michael H. Willemann

Graduate Knobler Scholars

Ted A. Asare
Feiming Bai
Todd M. Heil
Ben D. Poquette
Nurdan Demirci Sankir

Materials Science and Engineering
discover what we're made of...

Chris Kessler mounts wax parts onto a tree as part of the investment casting process. This was part of a foundry tour hosted by Conbraco.

Virginia Tech MSE students and faculty pause from a busy day at the American Ceramics Society Annual Conference in Baltimore, MD to enjoy lunch.

Holden Hall, the home of MSE at Virginia Tech.

The MSE soccer team poses for a group photo. Team membership is one of the many opportunities available through MEPS (Materials Engineering Professional Societies).

Materials students from Virginia Tech and the University of Florida teamed up to work as pages at the Cocoa Beach conference in Florida.

MEPS president Daniel Durrbeck and vice president Nicholas Bell take charge at one of the many MSE football tailgates co-sponsored by the College of Engineering.

Sophomore MSE students discuss heat treating options for 2024 aluminum that they will age harden for a laboratory class.

Mechanical Behavior of Nafion® and BPSH Membranes

Steven A. Kyriakides

Virginia Polytechnic Institute and State University
Department of Materials Science & Engineering
213 Holden Hall, Virginia Tech
*Blacksburg, Virginia 24061*

Abstract

A brief characterization of the mechanical behavior of Nafion® 117 and BPSH-35 membranes took place through uniaxial loading, stress relaxation, and creep compliance tests. Membranes were subjected to uniaxial loading at various strain rates to observe yield and fracture behavior. Stress relaxation tests measured relaxation response to strain rate and relaxation strain. Creep compliance tests led to the formation of a creep master curve for the Nafion® membrane. Tests showed that for Nafion®, higher strain rates produced higher yield stresses and yield strains as well as faster initial relaxation. Strain rate had no effect on strain at fracture. Higher relaxation strains also led to faster initial stress relaxation in both Nafion® and BPSH. BPSH results showed no yield trends in uniaxial loading, though they illustrated lower breaking strains with higher strain rates.

1. Introduction

Polymer electrolyte membrane (PEM) fuel cell research currently comprises a large portion of the search for alternatives to combustion engines.[1-7] Whereas combustion engines require combustion to convert chemical energy, these cells convert chemical energy directly to electrical energy via the following reactions:

$$2H_2 \rightarrow 4H^+ + 4e^- \qquad (1)$$

$$O_2 + 4H^+ + 4e^- \rightarrow 2H_2O \qquad (2)$$
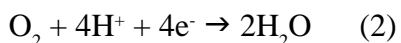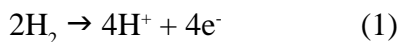
In PEM fuel cells, these reactions take place within the membrane electrode assembly (MEA), which consists primarily of a catalyst-coated polymer membrane, a cathode electrode, and an anode electrode. Hydrogen, either provided in pure form or extracted from another fuel, flows in on one side of the MEA. External air provides oxygen for the other side. The catalyst coatings, usually platinum, become an anode-cathode pair during the operation of the cell, with the reaction in Equation 1 taking place at the anode and that in Equation 2 taking place at the cathode. The flowing of the electrons produced from the anode reaction provides the electrical energy. The protons can pass through the polymer, at which point they combine with the oxygen and electrons to form water. This water, though a much more environmentally friendly byproduct than those produced by combustion engines, can lead to the failure of the entire fuel cell.

The polymers used for these fuel cells pose a problem in that that they will absorb some of the water produced during operation. This saturation alters the properties of the polymer, causing it to swell and produce compressive forces within the membrane. Prolonged swell-

ing initiates relaxation within the polymer. When the fuel cell stops running, the membrane will dry and contract, creating tensile stresses that lead to pinhole ruptures in the polymer. These pinholes effectively destroy the MEA, allowing the hydrogen and oxygen to interact freely without producing electrical energy.

Testing and analyzing the mechanical behavior of these membranes enables improved prediction and understanding of their failure mechanisms. The polymers studied in this project were the popular Nafion® 117, manufactured by DuPont, and BPSH, a potential direct methanol fuel cell alternative to Nafion® supplied by Dr. James McGrath of Virginia Tech.

Mechanical property tests were performed to measure tensile strength and stress relaxation patterns as a function of different strain rates. A dynamic mechanical analyzer (DMA) measured the creep compliance as a function of temperatures and the storage modulus as a function of frequency. Analysis of these results shows the membranes' responses to conditions within fuel cells at different stages of operation and fuel cell life.

2. Experimental Procedure

2.1 Materials

The Nafion® 117 (N117) extruded films had an equivalent weight (EW) of 1100 and a nominal thickness of 0.007 in. The BPSH-35 (BPSH) membrane had an EW of 770 and a nominal thickness of 0.005 in. Hydrosize Technologies, Inc. made the BPSH particles, which required dissolving, casting, and acidification to create the film and prepare it for testing. This material was completely amorphous at the onset of testing. Fuelcellstore.com sold the extruded N117 films, which required only acidification for testing. The extruded N117 is a semi-crystalline polymer, with the crystallinity dependent on the equivalent weight.[8]

2.2 Uniaxial Loading

Uniaxial loading tests were performed with samples prepared according to Figure 1 on an Instron 4468 Universal Testing Machine with a 1kN load cell.

Pneumatic grips held the 10mm segments at each end of the sample in the Instron machine under a 3 kg/cm^2 force. Strips of white reflective tape,

represented by the lines across the sample, created an extensometer gauge length of 10 mm. A Fiedler Optoelektronik GmbH laser extensometer measured the extension between the strips of tape. The partially reflective surface of the N117 produced some noise
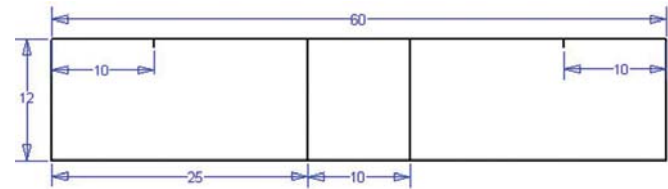
Figure 1. Uniaxial test samples (all dimensions in mm)

in the extensometer's results. The BPSH was so reflective that the extensometer could not differentiate between the membrane and the tape strips. Instead, the Instron machine's crosshead displacement was used to determine the BPSH extension. Samples underwent loading at strain rates of 0.025, 0.07, 0.12, 0.3, and 0.7 min^{-1}. Testing consisted of at least three N117 replicates for each strain rate and at least one BPSH replicate per strain rate.

2.3 Creep Compliance

Creep compliance tests were conducted using two TA Instruments 2980 Dynamic Mechanical Analyzers (DMA) using 6.5 by 26mm samples. With a preload force of 0.1 N and a stress of 0.5 MPa for N117 and 1.0 MPa for BPSH, the DMA measured creep compliance for two hours and the recoverable compliance for the subsequent two hours. The temperatures used for the N117 tests ranged from 10°C to 130°C in 10°C increments. BPSH test temperatures ranged from 150°C to 230°C, also in 10°C increments.

3. Results and Discussion

3.1 Uniaxial Loading

Figure 2 displays some of the results of the N117 uniaxial loading tests. This figure illustrates rising yield stresses and decreasing yield strains with increasing strain rate. This information, verified below in Table 1, agrees with the behavior described by Brown.[9] The Young's modulus for N117 remained roughly constant at 258 ± 8 MPa.

Figure 2. Nafion® 117 uniaxial loading test data

Table 1. Strain rate effect on Nafion® 117 yield strain and stress
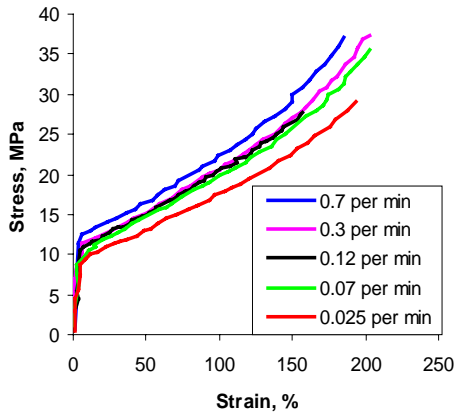
Strain Rate (min⁻¹)	Average Yield Strain (%)	Average Yield Stress (MPa)
0.7	8.05	12.66
0.3	8.3	11.57
0.12	8.775	10.59
0.07	9.13	10.50
0.025	9.45	9.946

Figure 3 illustrates the uniaxial loading results for the BPSH membranes. This figure shows a clear relationship between strain rate and strain at break. The higher the strain rate, the lower the breaking strain. The Young's modulus for BPSH, at 940 ± 20 MPa, was much higher and more variable than that of N117. BPSH begins its ductile fracture at far lower strains than the brittle N117 fractures occur.

As mentioned in the Experimental Procedure section, the laser extensometer determined the strain for N117 and the crosshead displacement was used to determine the strain for BPSH. This necessary change makes the exact values of the two membranes' strain measurements incomparable. However, the trends illustrated in the graphs above still hold true. Strain rate has a much larger effect on strain at break in BPSH than in N117. Regardless of strain rate, BPSH begins its ductile fracture at far lower strains than the brittle N117 fractures occur.

3.2 Creep Compliance

Though creep tests on N117 ran from 10°C to 130°C, thermal contraction at lower temperatures
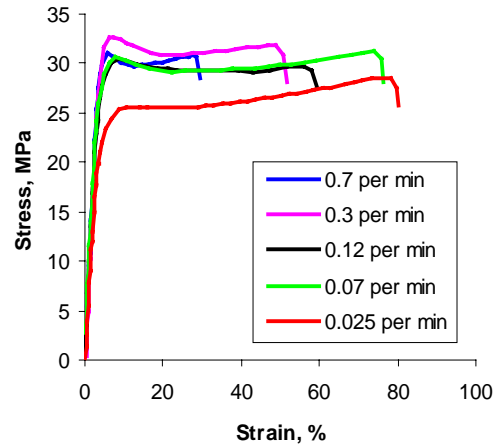
Figure 3. BPSH-35 uniaxial test data
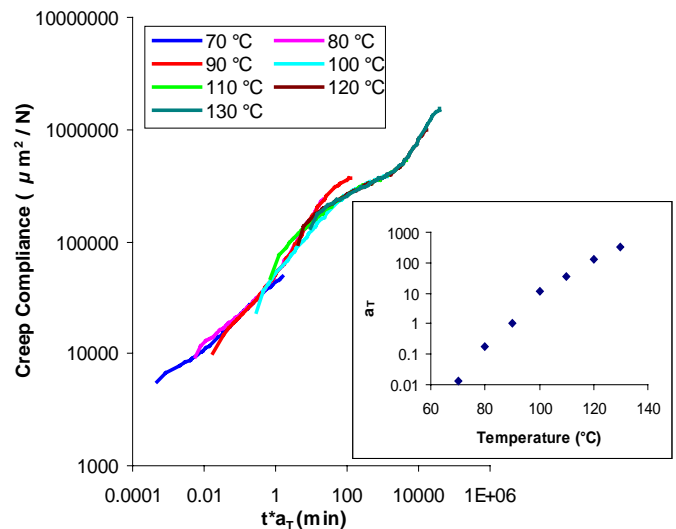
Figure 4. Nafion® 117 creep compliance master curve

tended to overwhelm the small stress used in the test, causing the sample to slowly contract instead of expand. The stress could not be increased, or else the sample would stretch farther at the higher temperatures than the instrument could measure. Since fuel cells typically run at roughly 60°C or more, the lower stress value was used. Figure 4 presents the master curve obtained from this test. The inset plot in Figure 4 shows the shift factor, a_T, used to generate the master curve.

For the same reasons as with the N117, BPSH creep tests could not produce accurate results at lower temperatures. Preload force values for the BPSH creep tests were the same as for the N117 tests. The data gathered was scattered and did not produce any

coherent master curve. Because of the high glass transition temperature (T_g) of BPSH, it was tested at a temperature range above that of N117; however, this high temperature range initiated decomposition in the samples, probably because water absorption at high temperatures lowered the T_g more than initially anticipated. This decomposition most likely caused the scatter in the data.

4. Conclusions

Uniaxial loading tests showed that for N117, higher strain rates lead to higher yield strains and yield stresses. Strain rate had no effect on the elongation at break for N117, but for BPSH, higher strain rates caused samples to fracture at lower strains. BPSH uniaxial test results illustrated no yield trends. N117 creep compliance data allowed for the creation of a reasonable master curve over the range of 70°C to 130°C. Due to some decomposition at high temperatures, BPSH creep data could not be used to produce a master curve. Additional mechanical testing is necessary to fully determine the possibility of replacing N117 with BPSH in fuel cell applications.

5. Future Work

Many other tests could be used to further characterize these membranes' mechanical behavior. Any or all of the above experiments could test response to varying equivalent weights. Stress relaxation and/or uniaxial loading tests could be conducted at varying temperatures. Uniaxial loading behavior in the transverse direction, as well as biaxial loading tests, could also be useful. A series of recovery and/or compression tests might also be helpful. In addition, the delamination of the polymers from the platinum catalysts could be modeled, since this is also a cause for the failure of fuel cells.

Acknowledgements

References

1. Fowler, M.; Mann, R.; Amphlett, J.; Peppley, B.; Roberge, P., Incorporation of Voltage Degradation into a Generalized Steady State Electrochemical Model for a PEM Fuel Cell. *Journal of Power Sources* **2002**, 106, 274-283.

2. Hickner, M.; Ghassemi, H.; Kim, Y.S.; McGrath, J., Alternate Polymer Systems for Proton Exchange Membranes (PEMs). *Chemical Reviews* **2004**, 104, (10), 4587-4611.

3. Jiang, R.; Chu, D., Voltage-time Behavior of a Polymer Electrolyte Membrane Fuel Cell Stack at Constant Current Discharge. *Journal Power Sources* **2001**, 92, 193-198.

4. Wilson, M.S..; Garzon, F.; Sickafus, K.; Gottesfeld, S., Surface Area Loss of Supported Platinum in Polymer Electrolyte Fuel Cells. *Journal of the Electrochemical Society* **1993**, 10, 140.

5. St. Pierre, J.; Wilkinson, D.P.; Knight, S.; Bos, M., Relationships between Water Management, Contamination and Lifetime Degradation in PEFC. *Journal of New Materials Electrochemical Systems* **2000**, 3, 99-106.

6. Markovic, N.; Ross, P.N., New Electrocatalysts for Fuel Cells from Model Surfaces to Commercial Catalysts. *Cattech*: **2000**; (2), 110-126.

7. Tazi, B.; Savadogo, O., Parameters of PEM Fuel Cells Based on New Membranes Fabricated from Nafion, Silicotungstic Acid and Thiophene. *Electrochimica Acta* **2000**, 45, 4329-4339.

8. Kyu, T.; Eisenberg, A., *Mechanical Relaxations in Perfluorosulfonate Ionomer Membranes. In Perfluorinated Ionomer Membranes; Eisenberg, A., Yeager, H., Eds.; A.C.S. Symposium Series 180*; A.C.S. Publishing: 1982, p 79-110.

9. Brown, N., *Yield Behavior of Polymers. In Failure of Plastics*. Brostow, W., Corneliussen, R., Eds.; Hanser Publishers: 1989; p 104-10.

Small Size Fluidic Devices by Freeform Manufacturing

Luis N. Folgar

Virginia Polytechnic Institute and State University
Department of Materials Science and Engineering
213 Holden Hall, Virginia Tech
Blacksburg, VA 24061

Abstract

The objective of this study was to innovatively use Freeform Manufacturing, specifically Selective Laser Sintering (SLS) to fabricate rapid prototypes of small size fluidic devices. The polymer used by the SLS application is very porous and presents a rough final surface. Material analyses were performed using Scanning Electron Microscopy (SEM), optical microscopy and Rockwell P hardness tests to develop methods for physical property enhancements. The study showed the feasibility of manufacturing a functional miniature size, e.g. sub-centimeter size, in-line static mixer derived from available macro-scale models using SLS and an additional coating process. It was determined that some of the variable parameters of the SLS process affected the mechanical and physical properties of sintered specimens. Related issues can be enhanced by sintering at relatively high laser power settings and post-processing the prototype with a polymer based coating.

1. Introduction

Industry has been continually changing techniques to produce mechanical work. Fluidic systems can be used to replace electrical systems in demanding applications for which they are not efficient. Already there are fluidic systems applications such as microanalysis systems, drug delivery devices, diagnostic tests, and fluidic biosensors. In this context, this study proposes manufacturing in-line static mixers by more automated means that can fit today's industries growing technological and economical needs. In-line static mixers are fluidic devices used in many applications such as drug delivery, food processing, pharmaceutical industry, toxic waste treatment, and water processing.

Solid freeform manufacturing, or freeform manufacturing (FFM), is a revolutionary technology used in building functional parts that can substitute production-quality parts[1,2]. This technology can automatically construct layer-by-layer physical models from computer-aided design (CAD) data. FFM involves many specific processes that take different names, and they are also often used as synonyms for the entire field of rapid prototyping. Selective Laser Sintering (SLS) was the manufacturing technique of choice for this project. Since the presented layer-by-layer manufacturing concepts and methods work for SLS, this feasibility can be expanded to many other FFM technologies

1.1 Materials and Technology Limitations

This project used EOS™ polyamide 2200 (PA) (Nylon 12), a material widely used in SLS applications. EOS™ PA has been developed specifically for creating rugged engineering thermoplastic parts that withstand aggressive functional test-

ing. EOS™ PA, however, has properties that may not be ideal for the manufacturing of functional prototypes of small size devices (i.e., porosity, surface roughness, low tensile strength). Currently, SLS is used in producing large scale three dimensional prototypes. This study suggests an in-line static mixer with dimensions reduced to a miniature scale. Sintering conditions can be varied to change mechanical properties of the sintered material. However, functional limitations for SLS units depend fundamentally on the laser beam width and layer thickness (step size).

2. Experimental Procedure

2.1 Computer Design of a Prototype

The areas involved in the prototype design were divided into CAD modeling, CAD files conversion, and model evaluation. The CAD model of an inline static mixer was developed in AutoCAD 2004®, taking reference specifications and designs from commercially available devices. To manufacture a prototype by SLS, the design files needed to be correctly formatted and evaluated. The models were created as solids and saved as CAD files (usually extension .dwg). The SLS files, however, are files of extension .stl, and therefore the CAD files need to be converted in order to be compatible with the software of the SLS unit. AutoCAD® allowed us to convert any file into .stl files as long as its contents were solids.

After the file conversion, the models were submitted to a pre-analysis and evaluation process performed by the software of the SLS unit. This evaluation stage was necessary because, once the process of building a prototype was in progress, design errors and adverse features could not be modified.

2.2 Material Analysis

Five samples were sintered using laser power settings of 4.5, 5.0, 5.5, 6.0, and 7.0 Watts respectively using a SinterStation 2000®. Each sintered sample was then subdivided into several specimens for further testing. Optical microscopy and Scanning Electron Microscopy (SEM) were used to assess surface roughness, porosity, sintering efficiency, and other unique microstructural characteristics of virgin powder and sintered specimens.

2.3 Material Properties Enhancement

The availability of many specimens made possible an extensive study of surface roughness enhancement of sintered samples at different intensities. Coatings of polyurethane and epoxy were then applied to the sintered sample specimens. Finally, SEM was used to identify which combinations of coating process and sintering conditions produced surfaces that were smooth and impermeable to liquids.

2.4 Hardness Testing

In order to examine the effect of varying the laser power settings, hardness testing was performed on EOS™ PA sintered samples at different intensities before and after the applied coatings. Hardness testing was performed using the Rockwell P scale which uses a 6.350 mm (1/4 in) ball indenter and a total test force of 150 kg to test very soft materials.[3] Micrographs of the respective indentations were compared to derive further correlations. A separate hardness testing was performed on a 16.51 cm long prototype specimen generally used for tensile testing (dog-bone sample). This sample was tested for hardness along the longitudinal axis with a spacing of 1 cm in between indentations.

3. Results and Discussion

3.1 SEM Results and Particle Size Analysis

Optical microscopy of powder EOS™ PA determined the particle size distribution to have an average of 60 µm. SEM studies performed on the EOS™ PA powder showed that the powder particles were generally uniform spheres or ellipsoidal. However, many of the particles displayed an opening in the middle cross-section with smaller particles visible within the crack-like feature (Figure 1). These smaller particles ranged from 2 to 7 µm and formed part of the larger particulate. The micrograph in Figure 1 revealed that our material is in fact formed by agglomerates of smaller particles (black arrows) and not single particles. Consequently, the remaining powder in sintered parts is due not only to limitations of the process, but also to incomplete sintering in the starting powder.

The phenomenon of partially sintered particles on the surface morphology of a sintered sample is illustrated in Figure 2. This problem results from the next-layer powder coming into contact with the sin-

tered layers before the material crystallization fully takes place in the consolidated matrix of the part under construction. The background of the micrograph (blue arrow) shows a matrix that indicates fully sintered EOS™ PA powder. This micrograph illustrates the presence of agglomerates (black arrows) with a crack-like feature even within the sintered matrix.

3.2 Surface Morphology of Samples

Stereomicroscopy analysis showed that the laser power settings have a significant effect on the surface morphology of sintered samples. The surface morphologies observed presented a uniform trend of
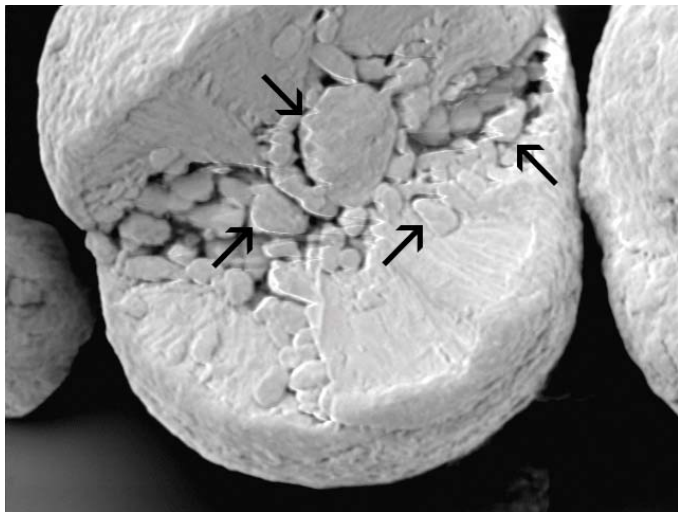

Figure 1. Scanning electron micrograph of powder EOS™ PA

having parallel lines of partially sintered material on the surface of the sample. These parallel lines run along the laser scan and sintering direction. It is very likely that non-sintered particles of material adhere to the surface of laser tracks after a scan of material has just been sintered. The variable widths between these parallel tracks suggested that the speed of the sintering laser beam was not uniform in the SLS system used. However, sintering efficiency was found to increase as the sintering laser power increased, and it was determined that a laser power of 7.0 W was optimal for building the prototypes.

3.3 Enhancement of Surface Morphology

The use of a polyurethane resin was found to be more suitable for enhancing the surface roughness of sintered EOS™ PA because of its low viscosity. This property allows an easy and practical application for faster results. Figure 3 shows SEM micrographs where coatings with epoxy resin present shattered glassy properties (Figures 3a and 3c). These features were not present when polyurethane resin was used. Polyurethane resulted in a smoother surface on samples sintered at higher power settings (Figure 3d).

3.4 Rockwell Hardness

Deformations from a stress are time-dependent for polymers because of the time it takes for their

Figure 2. SEM micrograph of sintered EOS™ PA

Figure 3. SEM micrographs of coated specimens sintered at different power settings

polymeric chains to unfold. The material's resistance to localized plastic deformation is therefore a time-dependent variable difficult to measure with precision. Due to this time-dep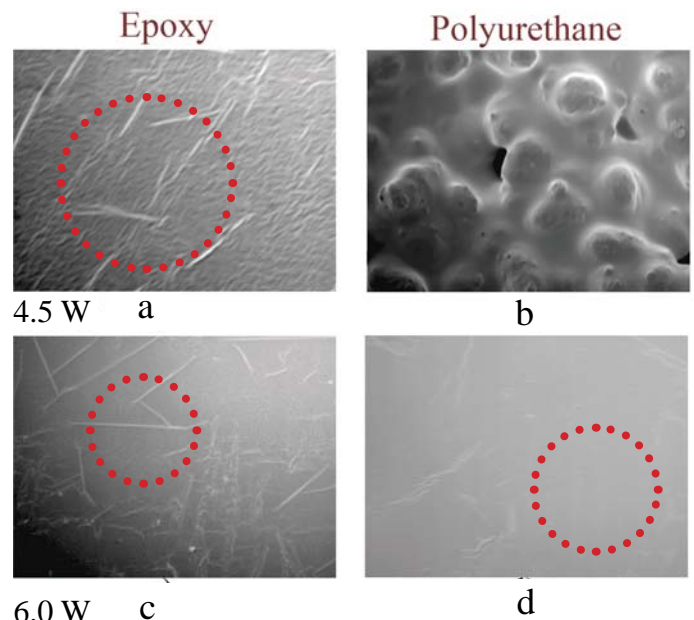endent response of the amorphous polymer used, the values found for hardness are considered to be only qualitative figures that show the trend that was found in the hardness behavior of the material. Therefore, the units for the hardness were determined to be arbitrary (au*) even though, as stated before, the P scale was used. Figure 4 illustrates the increasing values of hardness with increasing sintering-laser power. Coatings with polyurethane and epoxy increased hardness values. The coating with epoxy resin presented higher hardness values compared to polyurethane. Polyurethane resin was chosen over epoxy due to reasons previously stated.

Stereomicroscopy analysis demonstrated that indentation diameters on uncoated samples decreased as the laser sintering intensity increased. The inden-

tation diameters were approximately 2.87, 2.78, 2.71, and 2.55 mm for samples sintered at intensities of 4.5, 5.0, 6.0, and 7.0 W respectively.

The beam speed was found to be non-uniform, and scan space conditions, as stated before (Section 3.2), also affected the mechanical properties of the sintered material. Figure 5 shows that hardness values increased along the longitudinal axis from the center of the measured sample (dog-bone); the results of hardness to the left are almost a mirror image of the results for hardness values to the right. An explanation is that the heat of the build area including the sintered prototypes dissipates through the walls and the bottom of the SLS bed part. The resulting phenomenon is the presence of three-dimensional isotherms that induce differentials in material properties along the sintered segments (parts).[4] From this theory, it can be established that the shrinkage of a sintered part depends on temperature and time.

3.5 Stereomicroscopy Results

It was determined that the SLS system used was about 90% accurate in reproducing CAD models with their correct dimensions. This means that the SLS process presents a manufacturing technique capable of supporting designs with critical tolerances. Higher accuracy percentages can be achieved by having a better control and understanding of the variables that play a role in the SLS process. The final parts obtained were not functional devices, but they were demonstrational prototypes that proved the concept of the feasibility of manufacturing small size fluidic

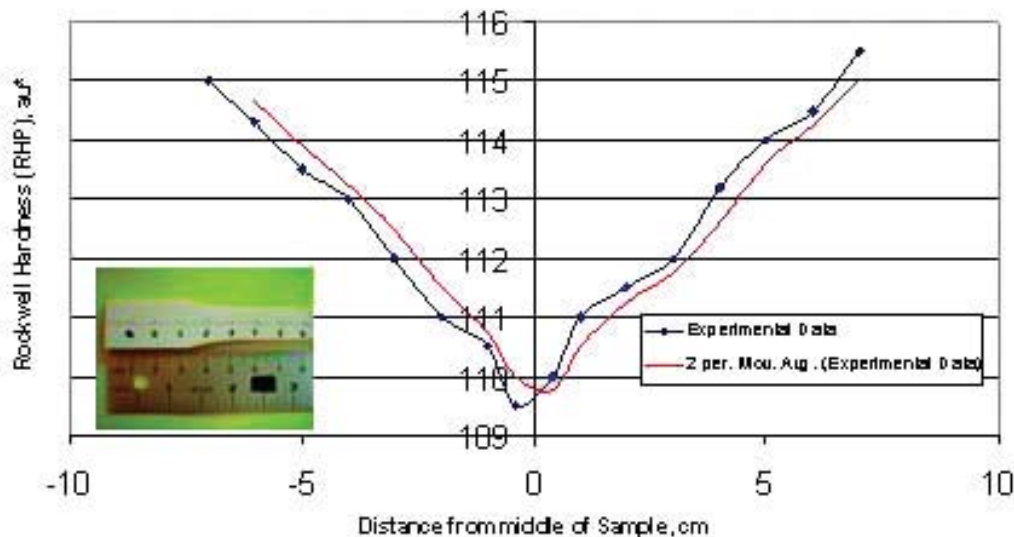Figure 4. Rockwell hardness values along the axis of a sintered sample

Figure 5. Rockwell hardness values along the axis of a sintered sample.

Figure 6. Small size in-line static mixer prototypes manufactured by SLS

devices by FFM. Figure 6 presents the manufactured in-line static mixers which are considered to be miniature size compared to the commercially available scales (~1-5m).

4. Conclusions

The performed research showed that it is feasible and practical to make prototypes of small size fluidic devices utilizing SLS. Once a CAD model of the fluidic device is drafted and converted to .stl format, an SLS unit can fabricate a three-dimensional prototype of the fluidic device. To make any prototype a functional device the optimal settings need to be determined because several factors affect performance and results. The effect of sintering laser beam speed, scanning space, and bed part temperature is worth noting in order to ensure the production of parts with uniform mechanical properties.

Raising the power of the sintering laser increased the efficiency of sintering nylon particles and reduced agglomerate nucleation sites. Rockwell P hardness tests also confirmed that raising the laser intensity increased strength. SEM and stereomicroscopy analyses confirmed that porosity and surface roughness were reduced when higher laser power settings were used during sintering. The coated prototypes of the miniature in-line static mixer were not tested for functionality. These prototypes were used for demonstrational purposes only. Finally, barriers such as the limited number of readily available materials for SLS still need to be overcome.

Acknowledgements

References

1. Das, S.; Beaman, J.J.; Wohlert, M.; Bourell, D. L., Freeform Fabrication of High Performance Titanium Components Via SLS/HIP. *Materials Research Society Symposium Proceedings* **1999**, 542, 45-50.

2. Zaw, H.M.; Fuh, J.Y.H.; Nee, A.Y.C.; Lu, L., Formation of a New EDM Electrode Material Using Sintering Techniques. *Journal of Materials Processing Technology Proceedings 4th Asia Pacific Conference* **1999**, 89, 182-186.

3. American Society for Testing and Materials. Annual Book of ASTM Standards; ASTM E18; ASTM Intl.: West Conshohocken, PA, 1998; 'Vol.' 3.01, p 180.

4. Shen, J.; Steinberger, J.; Gopfert, J.; Gerner, R.; Daiber, F.; Manetsberger, K.; Ferstl, S., Inhomogeneous Shrinkage of Polymer Materials in Selective Laser Sintering. *Solid Freeform Fabrication Symposium Proceedings* **2000**, 298-305.

A Novel Porous Polymers Manufacturing Technique

Erica L. Hartsell

Virginia Polytechnic Institute and State University
Department of Materials Science and Engineering
213 Holden Hall, Virginia Tech
Blacksburg, VA 24061

Abstract

There are many applications of porous materials, including the polymer, water, and metal filtration units of various industries; catalytic substrates; fuel cell components; surgical masks for doctors; "gortex" gloves for skiers; etc. In this paper, we discuss a novel method to make porous polymers. This method utilizes a mixture containing a biological agent (such as fungi) and a polymer. Characterization of the samples using the optical microscope and the scanning electron microscope (SEM) will also be discussed.

1. Introduction

Porous materials play a significant role in the international market and account for revenue totaling billions of dollars. The applications of porous materials are varied and include: thermal insulation, ion exchangers, filters and purifying systems, bone implants, Gortex clothing, catalytic substrates, porous battery electrodes, fuel cells, aerators, sorbents, silencers, kiln furniture, fiber optics, etc.[1-13]

Porous materials are characterized by their size distribution, shape, pore size, extent of interconnectivity and amount of porosity (open or closed).[8] The manufacturing techniques vary depending on the application for the porous material that is to be produced. For industrial applications, it is essential that the method chosen to produce the porous material is cost effective. This calls for developing novel techniques for the manufacturing of porous materials, especially porous polymeric materials.

In this paper, a novel technique to produce porous polymers using a biological agent is discussed. This method is based on the concept that a biological agent consists primarily of water, and if a the biological agent is dispersed in the polymer system, upon its death the biological agent will leave behind a pore in the material. Death of the agent occurs with time, by heating to elevated temperatures, or when the nutrient materials are exhausted. The size and shape of the pore will be that of the biological agent used. Here we discuss using a single celled fungus that is approximately one micron in size.

2. Experimental Procedure

2.1 Materials used

In this experiment, the polymer used was methylcellulose, commercially available from Dow. The biological agent used was a single celled fungus. The nutrient material needed for the single celled fungi to grow consisted of glucose ($C_6H_{12}O_6$) and de-ionized water.

2.2 Procedure

Measured amounts, 2 grams of the polymer methylcellulose, 1 gram of sugar, 2 grams of yeast, and 15 mL of water were used. The polymer (methylcellulose) was added with the de-ionized water after the water was heated to boiling. This was done to hasten the process of dissolution of the polymer. After the polymer dissolved in the liquid medium, the single celled fungi and glucose were added to this solution. The resulting mixture was allowed to dry for 48 hours. The pores in the samples were characterized using a scanning electron microscope (SEM).

3. Results and discussion

In the experiments, a biological agent (a single celled fungus) was used to generate pore in the structural material. The single celled fungus consumes glucose to grow and multiply. Upon consuming the glucose, the single celled fungus produces carbon dioxide gas and alcohol as waste. There are two mechanisms by which pores are generated in the material: the CO_2 gas produced creates pores, and the single celled fungi die leaving behind a pore, as they are comprised primarily of water. Equation 1 shows the reaction that takes place for the first case that was mentioned for the pore formation in the material.

$$C_6H_{12}O_6 \rightarrow 2C_2H_5OH + 2CO_2 \qquad (1)$$

SEM images were taken to show the porosity in the materials made using this new process. The size distribution and shapes of the pores are seen clearly. Figure 1 shows a sample of the porous polymer. We can see that many pores are smaller than 10 micrometers. Interconnectivity is evident from this view as the pores can be seen inside of the pore walls. Interconnectivity can be important for filtration and other applications. The pores in the range of a micron are caused due to the collapse of the biological agent. Figure 2 is another SEM micrograph of a sample. Here we can see the many pores along with the variation in size distribution and shape of the pores.

These images display a large amount of porosity in the material. It is hypothesized that with careful control of the nutrient media, and the biological agent being used (bacteria, viruses, protozoa, fungi, etc.), the drying methods, etc., will greatly influence the size and size distribution of the pores in the polymeric

structural material formed. This method can help reduce costs to make porous polymeric materials in industry. These biological agents are also relatively inexpensive.

4. Conclusions

A novel method for manufacturing porous polymers using a biological agent has been presented. A single cell fungus was used to form the porosity in the material. The porosity of the material has been characterized using the SEM.

Acknowledgements
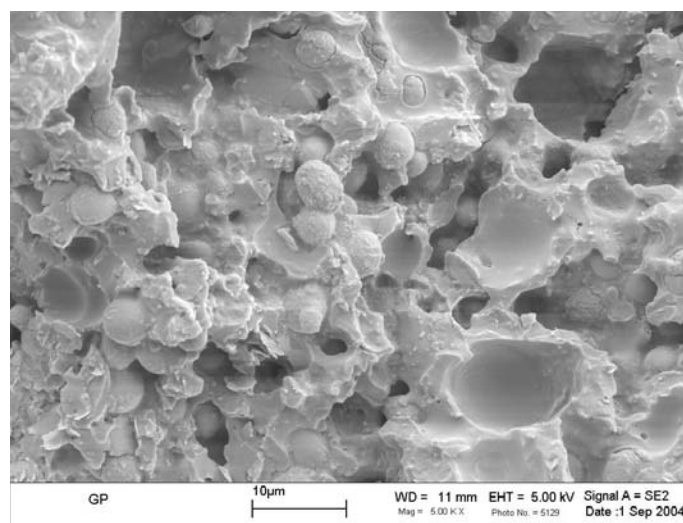
Figure 1. SEM micrograph of a porous polymer based structural material.
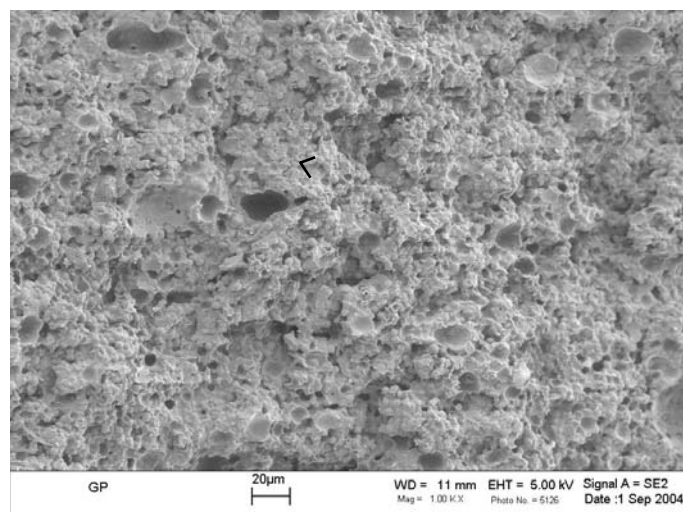
Figure 2. SEM micrograph showing pore size distribution.

References

1. Pickrell, G.R.; Butcher K.R., Method of Manufacture of Porous Ceramic Articles, US Patent 6210612, April 2001.

2. Pickrell, G.R.; Butcher, K.R., Porous Ceramic Articles, US Patent 6235665, May 2001.

3. Pickrell, G.R.; Butcher, K.R., Improved Porous Articles and Method for Manufacturing Thereof, US Patent 6592787, July 2003.

4. Welsh, G.; Ballot, M; Salmang, R., Process for Producing Thermo-formable Foam Sheet Using a Physical Blowing Agent, US Patent 200212716, 2002.

5. Sagui, C.; Picke, L.; Sahnoune, A.; Grant, M., Elastic Effects in the Foaming of Thermoplastics. *Physics Review E.* **1998**, 58 (4), 4654-4657.

6. Collington, K., A Preliminary Investigation of the Effects of Chemical Blowing Agents on the Physical Properties of Cellular Polymers. *European Journal of Cellular Plastics* **1978**, 1 (2), 107-113.

7. Liu, D.M., Porous Ceramics, in: *Key Engineering Materials, vol. 115*, TransTech Publications, Switzerland, 1996.

8. Rice, R.W., The Porosity Dependence of Physical Properties of Materials: A Summary Review, in: *Key Engineering Materials, vol. 115*, TransTech Publications, Switzerland, 1996; p 1-20.

9. Zievers, J.F.; Eggerstedt, P.; Zievers, E.C., Porous Ceramics for Gas Filtration. *American Ceramics Society Bulletin* **1990**, 70 (1), 108-111.

10. Lang, F.F.; Miller, K.T., Open-Cell Low-Density Ceramics Fabricated from Reticulated Polymer Substrates. *Advanced Ceramic Materials* **1987**, 2 (4), 827-831.

11. Butcher, K.; Pickrell, G., A New Generation of Ceramic Foams with Small Pore Size, in: Lednor, P.W.; Nagaki, D.A.; Thompson, L.T. (Eds.), *Advanced Catalytic Materials, vol. 549 of the Materials Research Society Proceedings Series*, Materials Research Society, 1999; p 9-16.

12. Minnear, W.P., Processing of Foamed Ceramics, in: M. Cima (Ed.), *Ceramic Transactions, vol. 26*, American Ceramic Society, 1992; p 149-156.

13. Pickrell, G.; Peng, W.; Wang, A., Random-hole Fiber Evanescent Wave Gas Sensing. *Optics Letters.* **2004**, 29 (13), 1476-1478.

The Effect of Viscosity and Ion Size on the Transduction of Ionic Polymer Metal Composite Actuators

Lisa A. Copley, Elizabeth D. Hubbard, and Adam J. Maisano

Virginia Polytechnic Institute and State University
Department of Materials Science and Engineering
213 Holden Hall, Virginia Tech
Blacksburg, Virginia 24061

Abstract

Ionic polymer membranes plated with platinum and gold serve as actuators when a small potential is applied. However, the water used to hydrate the membrane evaporates during use, decreasing actuator performance. Ionic liquids are being considered as a replacement for water because of their low vapor pressure. Prior studies show that the large ion size and high viscosity of ionic liquids slow the response time of the polymer membrane when a voltage is applied. This study examines the relationships of ion size and viscosity to transduction by modeling ionic liquids with inexpensive salts of varying ion size and glycerol/water solutions. Based on these results several ionic liquids were selected and tested for use as membrane solvents. This study includes frequency response, step response, and impedance tests of samples impregnated with Li^+, K^+, Cs^+, TMA^+, TEA^+, and TBA^+. Actuators solvated in solutions with a viscosity similar to 70–80 wt. % glycerol solutions (18–46 cP) and cation size similar to that of TMA^+ (0.347 nm) appear to yield the best results. When used as the membrane solvent, the ionic liquid 1-ethyl-3-methyl imidazolium trifluoromethanesulfonate (IL #3) resulted in the greatest strain per charge per area of the three ionic liquids tested in this study.

1. Introduction

Ionic polymer metal composites (IPMCs) are smart materials being investigated for applications as actuators and sensors. These materials require low operation voltages of 1–5 V and act as simple mechanical devices. When an electric field is applied across the IPMC, the movement of cations and water molecules inside the membrane causes the actuator to bend toward the anode. Optimum transduction occurs when an actuator exhibits maximum deflection, quick response time, and no back relaxation toward the original position after deflection. IPMCs act as transducers because they convert electrical energy to mechanical motion, or vice versa.

The IPMCs are manufactured by plating an ionic polymer membrane with a thin layer of metal. The majority of work in this area uses a Nafion™ polymer membrane plated with a thin layer of platinum metal, then with a layer of gold metal to improve surface conductivity.[1, 2] Previous work established a procedure for manufacturing IPMCs with repeatable mechanical and electrical properties.[1]

The degree of hydration of the polymer is critical to membrane transduction, but previous work has been limited by the evaporation of the water from the membrane during testing. This dependency on hydration limits the applications of IPMCs to aqueous environments.[3] Ionic liquids are being considered to replace water as the IPMC membrane solvent, which would extend their use to non-aqueous environments. Some potential applications for the actuators are heart-assist devices, catheter guidance, and blood pressure measurement devices.[4]

Ionic liquids are room temperature molten salts made up of dissociated cations and anions.[5] These liquids have low vapor pressure at room temperature and therefore evaporate more slowly than water. It is estimated that approximately one trillion room-temperature ionic liquids exist.[6]

Preliminary experiments using ionic liquids as membrane solvents show that transduction and the resulting deflection occur more slowly than when water is used. Slow actuation may result from the viscosity of the solution and the relatively large ion size. Seven ionic liquids were selected for characterization and evaluation on the basis of similar cation and anion combinations. The seven ionic liquids chosen were:

- tetramethylammonium bis(trifluoroethyl)imide
- tetramethylammonium tris(pentafluoroethyl) trifluorophosphate
- 1-butyl-1-methylpyrrolidinium bis(trifluoromethylsulfonyl)imide
- 1-butyl-1-methylpyrrolidinium tris(pentafluoroethyl) trifluorophosphate
- trihexyl(tetradecyl)phosphonium bis(trifluoromethylsulfonyl)imide
- trihexyl(tetradecyl)phosphonium tris(pentafluoroethyl) trifluorophosphate
- 1-ethyl-3-methylimidazolium trifluoromethansulfonate

2. Procedure

The use of ionic liquids as membrane solvents in IPMCs has only recently been studied, and the characterization of the effects of using ionic liquids is not well documented. These liquids have a large range of viscosities and ionic radii, both of which are thought to have an effect on the transduction of IPMCs. Therefore, this study used membrane solvents of varying viscosity and ion size to model the effects on the transduction of IPMCs to help determine an optimum range of viscosity and ionic radius for selecting an ionic liquid.

Six salt solutions were mixed using lithium (Li^+), cesium (Cs^+), potassium (K^+), tetramethylammonium (TMA^+), tetraethylammonium (TEA^+), and tetrabutylammonium (TBA^+) as the cations and water as the solvent. A sheet of platinum-plated and gold-plated Nafion™ was cut into 36 specimens measuring 4 by 35 mm. Six IPMCs were placed in each of the salt solutions and put into an oven at 100°C for two days. Several days prior to testing, the six IPMCs in each salt solution were removed from the solution and dried for 48 hours at approximately 80°C between steel plates with copper spacers. Six glycerol and water solutions of 0, 60, 70, 80, 90, and 100 wt. % glycerol were produced to effectively study a range of different viscosities. After verifying the six solution viscosities using a Brookfield DV-II+ viscometer, published values were used for the remainder of the project.[7] One cation-impregnated IPMC was placed into each glycerol solution and held at 100°C for 24 hours. This resulted in 36 samples impregnated with six cations and solvated in six fluids of varying viscosity.

3. Results and Discussion

3.1 Frequency Response Characterization

Frequency response tests conducted on each of the 36 samples measured voltage, current, and tip displacement to determine the strain, impedance, and capacitive properties of IPMCs when a random voltage is applied. Figure 1 shows the frequency response test data for TMA^+ as a representative sample of results for all sample sets. Figure 2 contains the frequency response test data for the 70 wt. % glycerol samples as a representative sample for all the sets.

The displacement was calculated with the laser output data and the laser gain setting. The impedance at a given frequency was determined by calculating the resistance, R, from the measured current, I, and voltage input, V, according to Equation 1.
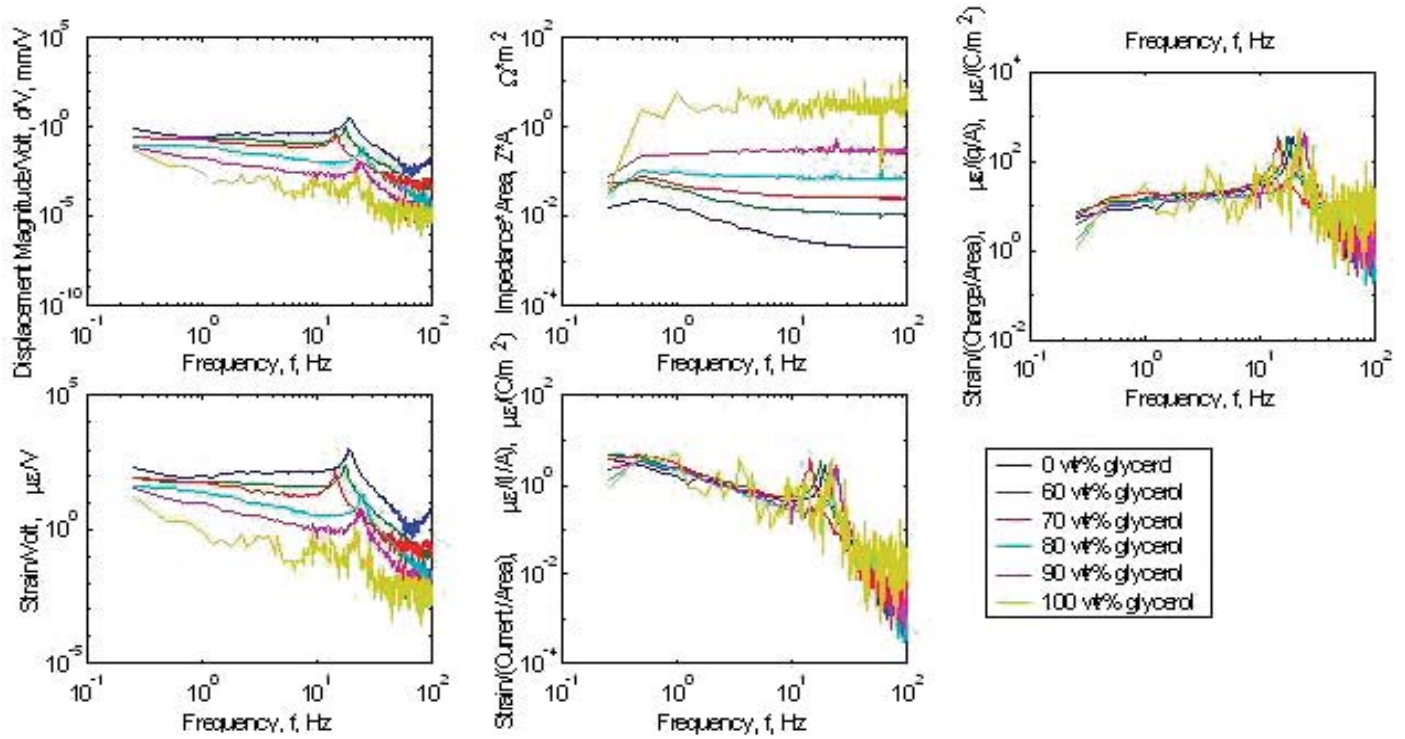
$$R = \frac{V}{I} \tag{1}$$

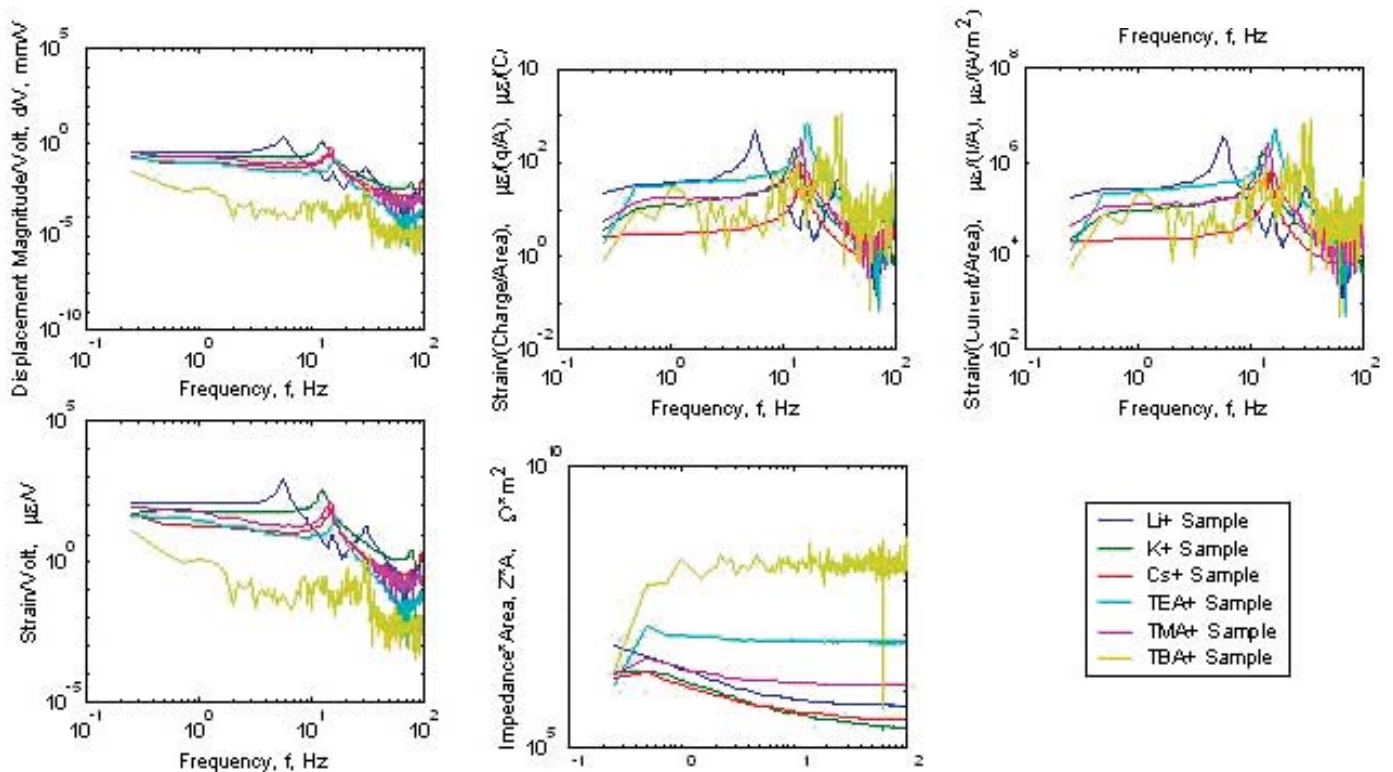**Figure 1. Frequency responses of TMA+ samples**

Figure 2. Frequency responses of 70 wt. % glycerol samples

Constant impedance indicates that the actuator behaves as a resistor. The resistance is due to the low mobility of the large cations through the membrane. However, smaller cations, such as Li^+ or K^+, behave as capacitors, as indicated by the negative slope of impedance.

$$Strain = \frac{Displacement \times t}{L^2} \quad (2)$$

The strain was determined by multiplying the magnitude of displacement by a geometric factor in Equation 2, where t is the sample thickness and L is the length of the actuator. The strain per current at a given frequency was determined by multiplying the strain by the impedance. The strain per charge at a certain frequency was calculated by multiplying the strain per current by ω, the angular frequency, in Equation 3.

$$\omega = 2\pi f \quad (3)$$

The impedance is consistently higher for samples with more viscous membrane solvents, as shown in Figure 3. The impedance of the samples impregnated with TBA^+, the largest cation, is less sensitive to changes in viscosity than those impregnated with smaller cations, such as Cs^+ or K^+. This trend is shown by the constant impedance for TBA^+ as a single frequency in Figure 3.

Ionic polymers with lower viscosity membrane solvents and small cations deflect the largest distance and result in the greatest amount of strain at low frequencies as shown in Figure 4. The strain measured on IPMCs impregnated with TBA^+ is less dependent on solvent viscosity than for the IPMCs impregnated with smaller cations. As shown in Figure 5, the cations with radii less than approximately 0.45 nm have

Figure 4. Strain/volt at 2 Hz vs. viscosity

be compared directly. These data suggest that once charge is stored in the actuator, the electromechanics are very similar, regardless of solvent viscosity or ionic radius, and indicate that differences in actuation are a function of the electrode

3.2 Ionic Liquids

Based on the evaluation of transduction using various viscosities and ion sizes, actuators with a viscosity similar to 70–80 wt. % glycerol solutions and cation size similar to that of TMA^+ appear to yield the best results. The viscosities of the three ionic liquids evaluated range from 35 to 224 cP. The viscosities of 70 and 80 wt. % glycerol solutions at room temperature are 18 cP and 46 cP, respectively. Frequency
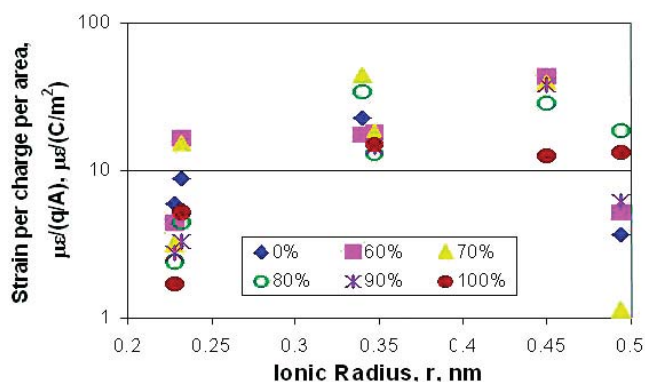
Figure 5. Strain/(charge/area) at 2 Hz vs. ionic radius

response tests were performed on actuators solvated in the following ionic liquids (IL):

- 1-butyl-1-methyl pyrolidinium bis(trifluoromethylsulfonyl)imide (IL #1)

Figure 3. Impedance*area at 100 Hz vs. viscosity

- 1-butyl-1-methyl pyrolidinium tris(pentafluor-oethyl)trifluorophosphate (IL #2)
- 1-ethyl-3-methyl imidazolium trifluoromethanesulfonate (IL #3)

The results of these tests are shown in Figure 6. IL #3 was impregnated with H^+ and Li^+, while IL #1 and IL #2 were only impregnated with H^+. The viscosities for IL #1, IL #2, and IL #3 are 76 cP, 224 cP, and 35 cP, respectively.

Actuators solvated in ionic liquids have electro-mechanical properties similar to actuators solvated in glycerol solutions of comparable viscosity, as shown in Figure 3. Although the exact ionic radii of the ionic liquids tested are unknown, the cations in the liquids are large, and their frequency response behavior can help predict the ionic radii based on preliminary experimental data using various cation sizes. Figure 6

shows a plot of the frequency response test data for the three ionic liquids.

Actuators solvated in IL #1 and IL #2 behave in the same manner as actuators impregnated with large ions, such as TBA^+. Although the viscosity of IL #1 was much lower than that of IL #2, the strain per charge per area plots of the two actuators are approximately the same. This agrees with the trend noted in the preliminary testing, which indicates that as the cation becomes larger, the strain and impedance of the actuator become independent of viscosity. The behavior of the two actuators solvated in IL #3 is similar to those impregnated with TMA^+ and TEA^+. The impedance per area for both of these actuators is low, indicating capacitive characteristics. The strain per charge per area plots give smooth curves with resonant frequencies resembling those of TMA^+.

Figure 6. **Frequency responses of ILs**

4. Conclusions

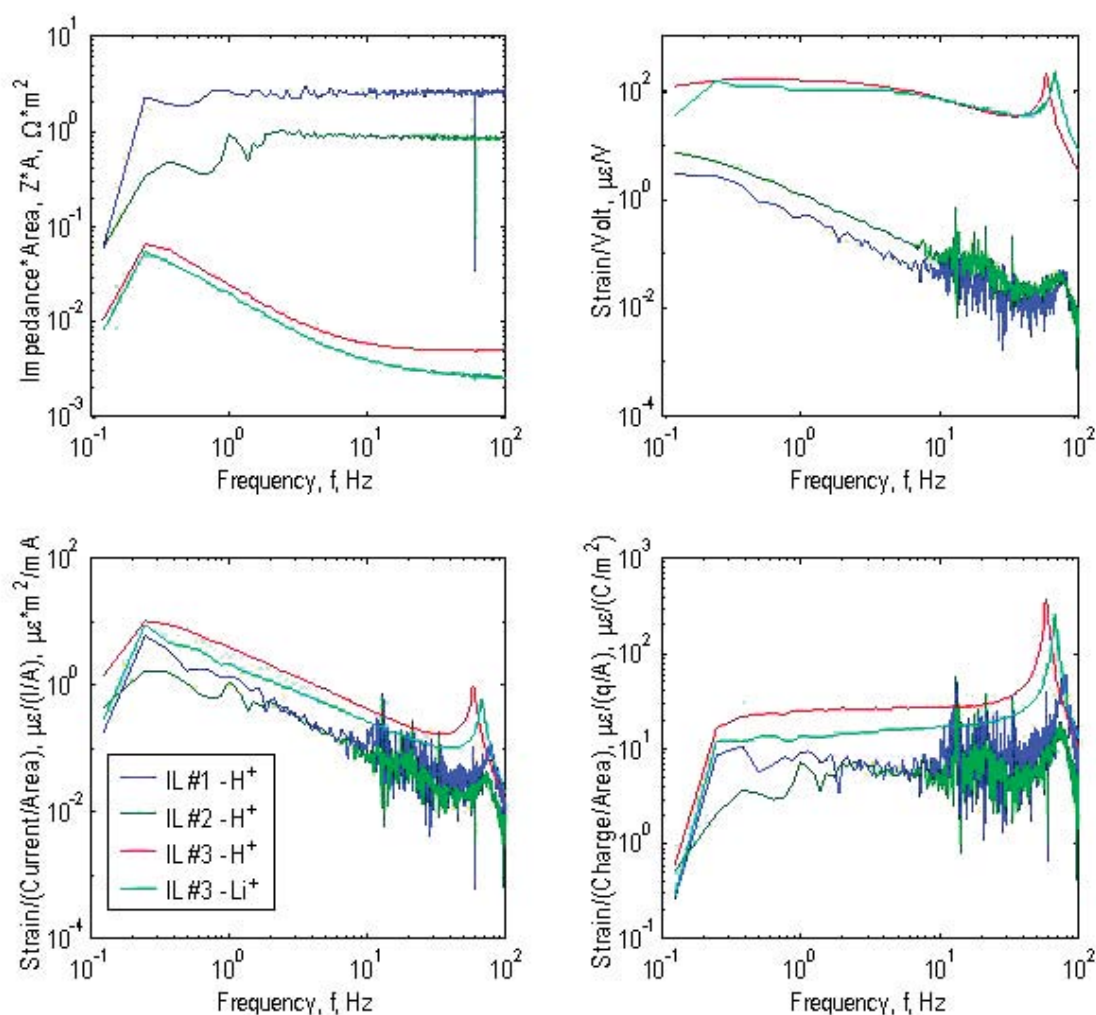The results of the study indicate that ionic liquids may be suitable replacements for water as the membrane solvent. Of the three different ionic liquids tested as membrane solvents, those exhibiting successful frequency response data had cations approximately the size of TMA$^+$ and viscosities near that of 70 to 80 wt. % glycerol. Therefore, the most effective ionic liquids were characterized by an ionic radius of approximately 0.347 nm and a viscosity between 18 and 46 cP. Actuators solvated in ionic liquids with these characteristics had low impedance and high strain per charge per area. These actuators stored charge and current flowed through the membrane, causing a displacement.

Based on the frequency response testing, viscosity played a larger role in the transduction when smaller ions were used to impregnate the polymer. The smaller ions possessed greater mobility inside the polymer membrane, allowing transduction to occur more easily. Similarly, the larger ions were less dependent on viscosity because their bulky size limited movement inside the polymer membrane. As the ionic radius of the cation increased, the deflection and resulting strain decreased. Additionally, the IPMCs impregnated with larger cations had higher impedance. Increasing viscosity resulted in higher impedance of the IPMC. Small ion size and low viscosity would produce the IPMC with the most favorable frequency response.

Acknowledgements

References

1. Bennett, M. D; Leo, D. J., Manufacture and Characterization of Ionic Polymer Transducers Employing Non-Precious Metal Electrodes. *Smart Materials and Structures* **2003**, 12, 424–436.

2. Nemat-Nasser, S., Micromechanics of Actuation of Ionic Polymer-Metal Composites. *Journal of Applied Physics* **2002**, 92 (5), 2899–2915.

3. Knechel, J.; Love, C.; Whited, B., Improving Repeatability of Cu/Pt Ionic Polymer Metal Composite Actuators. Senior Design Project Report, Materials Science and Engineering Department, Virginia Tech, 2003.

4. Newbury, K., Characterization, modeling, and control of ionic polymer transducers. Ph.D. Thesis, Virginia Tech, 2002.

5. Xu, W.; Cooper, E. I.; Angell, C. A., Ionic Liquids: Ion Mobilities, Glass Temperatures, and Fragilities. *Journal of Physical Chemistry* **2003**, 107, 6170–6178.

6. Gorman, J., "Faster, Better, Cleaner?" Science News Online. 8 Sept. 2001.

7. Miner, C. S.; Dalton, N. N., *Glycerol*. Reinhold Publishing Corporation: 1953; p 278–287.

Characterization of the Effect of Film Thickness on the Electrochemical Impedance of Nanoporous Gold

Nicholas C. Bell, **James G. Collins**, and **Ryan M. Turner**

Virginia Polytechnic Institute and State University
Department of Materials Science and Engineering
213 Holden Hall, Virginia Tech
Blacksburg, Virginia 24061

Abstract

Graphs are generated characterizing the effect of film thickness on the electrochemical impedance of nanoporous gold. Twelve-karat white gold (50% Ag, 50% Au) leaves were dealloyed to make a total of 12 nanoporous gold samples from 100-300 nm thick. Scanning electron microscopy (SEM) was used to determine the pore diameter distributions and an electrochemical cell was used to collect impedance data for each sample. Analysis of the SEM micrographs shows the pore morphology ranges from shallow spherical pores to deep interconnected pores, and the diameter distributions were between 10 nm and 20 nm for all of the samples. A linearized graph of impedance |Z| versus frequency shows that the breakpoint frequency decreases with increasing film thickness. Below the breakpoint frequency, the data support an idealized model that assumes through-thickness pores with uniform diameters. Above the breakpoint frequency, however, the ideal model predicts a drastic impedance decrease, whereas the data show only a slight impedance decrease.

1. Introduction

Industry currently uses nanoporous metals in several applications, such as leads in cardiac pacemakers, because they provide large surface area at reduced material mass. For example, cardiac pacing leads are coated with a nanoporous metal layer that conducts electrical signals to the heart through saline-like body fluids.[1,2,3] These metals have relatively high electrical impedances that lower the stimulating current to the heart. Little is understood, however, about the effect of film thickness on the leads' electrical properties, such as impedance. Current literature about nanoporous metals discusses only the composition and dissolution potential necessary for creating pores.[4,5,6] Characterizing the effect of film thickness on a nanoporous metal's electrochemical impedance could help manufacturers control performance characteristics such as longevity more closely.

1.1 Nanoporous Gold

Although platinum is a typical component of pacing leads, gold provides a nanoporous model analogous to a platinum system. Gold is a model alloy system composed of a single phase alloy over the entire composition range, with

only 0.2% lattice misfit between Ag and Au. This low misfit allows structural changes to be ignored when Ag is selectively dissolved from Au in dealloying.[3] Additionally, gold is less expensive than platinum and is readily accessible and much easier to process, making it ideal for preliminary modeling.

Nanoporous metals used for cardiac pacing leads are produced through dealloying, in which the most electrochemically active element of an alloy is parted through selective dissolution.[1,2,4-7] This selective dissolution produces a sponge-like nanoporous structure of the more noble alloy element.[5] Early in the process of dealloying silver from an Ag-Au alloy, the gold clusters form mounds with gold-rich peaks on the surface and bases that resemble the starting alloy. Further dissolution attacks the bases of the mounds and creates pits that contribute to the nanoporosity of the alloy.[1,5,6]

1.2 Impedance Theory

Impedance is a material's ability to slow down the flow of electrical current. For pacemaker applications, higher lead impedance lowers the current needed to stimulate the heartbeat, which extends the battery life. Equation 1 shows the relationship between

$$I_l = \frac{V_0^2 t}{V_b Z_p L} \qquad (1)$$

pacing impedance and current seen by the patient: where I_l is the current delivered to the patient, Z_p is the pacing impedance, V_o is the output voltage, V_b is the battery voltage, t is time, and L is cycle length.[1] The battery produces an alternating current (AC) of varying frequencies, and the frequency depends on pore size, shape, and distribution for nanoporous metals.[1] Therefore, impedance depends on porosity.

The breakpoint frequency is the frequency at which the current passes through the pore surface area of the nanoporous metal, and the metal no longer acts like a continuous, polished material. Because apparent surface area in the nanoporous metal increases substantially, impedance rises sharply as frequency decreases. However, above the breakpoint frequency, the current passes over the lead as though it had a polished surface and consequently lowers the overall impedance of the lead.[1] In addition, increasing porous layer thickness will decrease the lead's impedance and shift the breakpoint frequency to a smaller value.[1] Lowering the breakpoint frequency

allows a lower AC current frequency to be used to achieve a given impedance compared to nanoporous materials with higher breakpoint frequencies or polished, continuous materials.

To facilitate control of impedance characteristics, this research analyzes the effect of film thickness on the electrochemical impedance of nanoporous gold. Changes in breakpoint frequencies for various film thicknesses were analyzed to determine a procedure for lowering the breakpoint frequencies of nanoporous gold and to model this effect to predict impedance behavior for other film thicknesses.

2. Experimental Procedure

2.1 Nanoporous Gold Sample Preparation

Each nanoporous gold sample was made by dealloying 12-karat, 100 nm thick Monarch white gold leaf (50 wt. % Au, 50 wt. % Ag) manufactured by Sepp Leaf Products, Inc. First, the leaf was rolled onto a graphite rod and unrolled into a dish of de-ionized (DI) water to make the leaf taut. After rolling the leaf back onto the graphite rod, it was unrolled into a dish filled with 0.1 M HNO_3 and allowed to dealloy for five minutes.

Next, the nanoporous foil was rolled onto the graphite rod and unrolled into a dish of DI water. Foil transfer from one DI water bath to another continued four more times for thorough foil washing. Then, a piece of clean silicon wafer was submerged beneath the foil and lifted out of the DI water with some of the foil adhered to it, after which the foil was dried to the wafer in a general purpose Precision™ oven at 145°C for 10 minutes. Sample thicknesses were produced with thicknesses of 100 nm, 200 nm, and 300 nm. Film thickness was increased by adding another gold foil to a foil already adhered to a silicon wafer. The use of silicon wafers with oxide layers was avoided because oxide layers prevent film thickness stacking. Since heating silicon wafers creates oxide, unnecessary sample heating was avoided as well. Overall, a total of 12 samples were created with four samples for each film thickness.

Scanning electron microscopy (SEM) specimens were prepared by using a diamond-tipped scriber to remove a small section from each sample. The SEM specimens were viewed using a LEO® 1550 SEM at

a magnification of 300k with an accelerating voltage of 5 kV. All samples were stored in a humidity-controlled nitrogen cabinet.

2.2 Electrochemical Impedance Testing

Electrochemical impedance tests were performed on samples not viewed with SEM using a three-electrode electrochemical cell set-up at room temperature. A KIMAX® crystallizing dish with a 170 mL maximum capacity was filled about ¾-full with 0.1 M $HClO_4$. The dish was placed on a platform lift on the base of a stand. Alligator clips attached to a Gamry® Potentiostat were suspended from the stand's clamps. A saturated mercury/mercurous sulphate (MSE) reference electrode was suspended from one clamp, whereas a platinum foil counter electrode was attached with an alligator clip to another clamp. A copper lead was attached to the sample to be tested using Teflon tape with the lead making sufficient contact with the nanoporous gold foil to create the third electrode.

Using the platform lift, the dish containing the $HClO_4$ was raised to submerge all three electrodes in the acid. Before submerging the sample, the surface area of the part of the sample to be tested was approximated with a caliper, and the edges of that area were covered with a small amount of DI water to ensure that the $HClO_4$ did not peel the foil from the wafer as it submerged. Each test was run using Gamry Instruments® Framework 3.20 electrochemical testing software. First, the DC voltage potential was held at the open circuit potential while an AC potential of 10 mV rms was applied across that part of the sample submerged in the $HClO_4$. After entering the approximated surface area, the impedance test ran from frequencies of 0.2 to 1E6 Hz. The results were viewed using ZView 2.3d (by Scribner Associates, Inc.) from which the data were extracted and imported into spreadsheet software for analysis.

2.3 Data Analysis

Pore diameter distributions were determined by using image threshold software on the SEM micrographs. The software creates a dark/light contrast between the pores and the ligaments, measuring the diameter of the dark areas (the pores). The results were used to create histograms showing the pore diameter distributions.

Graphing software was used to generate graphs of the impedance magnitude |Z| (ohms) versus frequency (Hz) in log-log coordinates for each film thickness to estimate where each curve's slope changes (i.e., the breakpoint frequency). The impedance data were imported into spreadsheet software, which was used to calculate the average |Z| for each film thickness. The point-slope method was used to create a linear curve with a distinct slope change for each film thickness. A more specific breakpoint frequency exists where the slope changes for each curve. The spreadsheet software was also used to calculate the standard deviation between the breakpoint frequencies of the samples for each film thickness.

3. Results and Discussion

3.1 SEM Micrographs of Pore Morphology

SEM micrographs of each sample were obtained to confirm pore morphology and distribution of pore sizes in the nanoporous gold. Pore morphology ranges from roughly spherical pores to interconnected pores, as seen on the surface of the 100 nm thick sample shown in Figure 1. Figure 2 is the pore size distribution for a 100 nm thick gold sample and indicates the pore sizes are in the expected range for a dealloying time of 5 minutes in HNO_3.

The majority of the pore diameters fall between 10 nm and 20 nm. SEM micrographs and pore size distributions of the 4 samples for each thickness (100 nm, 200 nm, 300 nm) indicate a consistent pore diameter and pore morphology among all 12 samples.
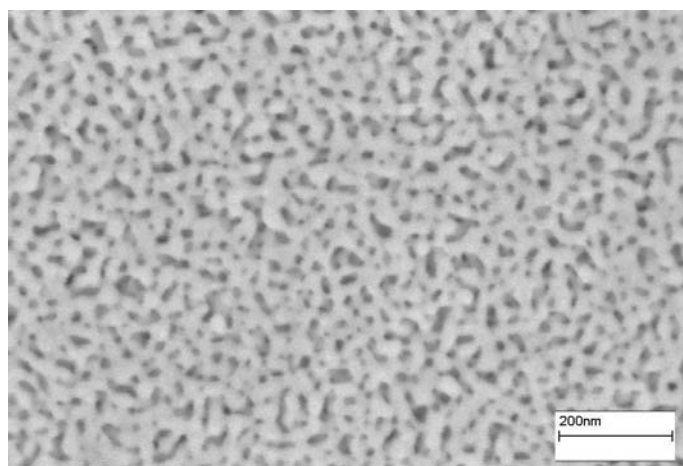

Figure 1. SEM micrograph of a 100nm thick nanoporous gold sample on a Si [110] substrate

3.2 Film Thickness Effects on Breakpoint Frequency

Figure 3 plots the average |Z| versus frequency of the four samples tested for each film thickness, showing a distinct slope change between the background (the region of the curve at the lower frequencies) and the foreground (the region of the curve at the higher
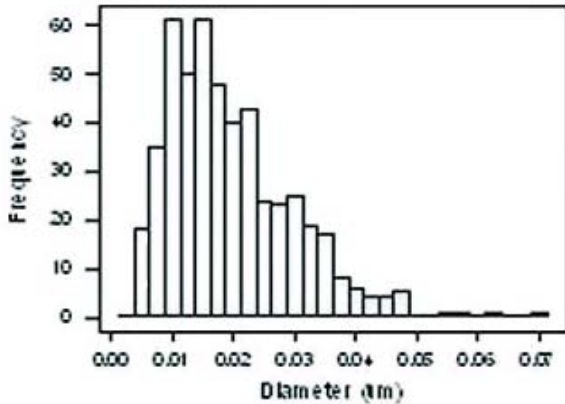

Figure 2. Pore size distribution of a 100 nm thick nanoporous gold sample on a Si [110] substrate

frequencies). Figure 4 displays a linearized version of Figure 3 in which the linearity of the background and foreground for each curve is enhanced to find a specific breakpoint frequency, denoted by the circles. Overall, Figure 3 shows that an inverse relationship exists between film thickness and breakpoint frequency for nanoporous metals: as film thickness increases, breakpoint frequency decreases.

The average breakpoint frequencies are 34.0, 28.5, and 11.98 Hz for the 100 nm, 200 nm, and 300 nm film thickness, respectively. The standard deviation
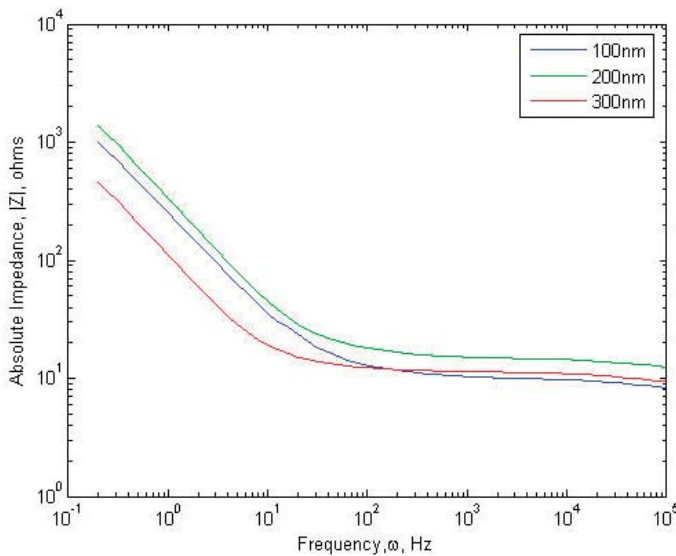
Figure 3. Real impedance vs. frequency data
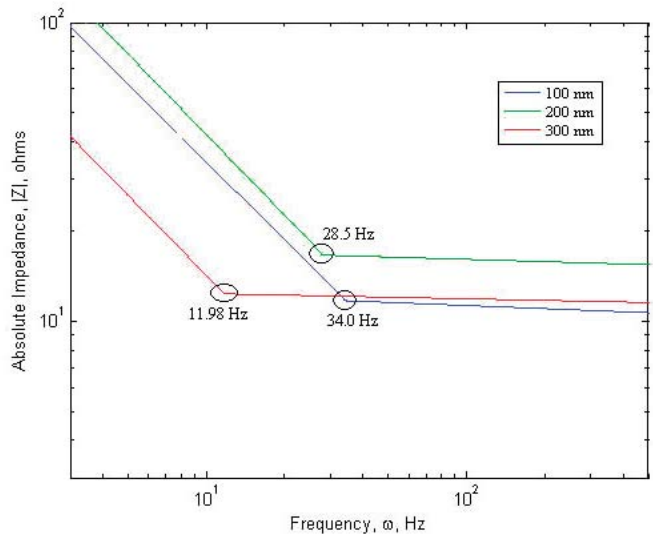
Figure 4. Calculated breakpoint frequencies for real impedance data

is 7.4, 2.1, and 1.3 Hz for the 100 nm, 200 nm, and 300 nm film thickness, respectively. Consequently, the 100 nm data range overlaps that of the 200 nm film thickness. Additional testing should decrease the standard deviation of the 100 nm film thickness data and refine the model.

3.3 Comparison to Existing Models

The ideal model from Dr. Pugh's thesis[1] (and shown in Figure 5) was based upon the De Levie equation typically cited in literature. It suggests that as film thickness increases, the breakpoint frequency decreases. Our data agree with this theory in that below the breakpoint frequency, the electrical current passed through the entire surface area including the pores, thus increasing impedance. However, our high-frequency data disagree with that of the ideal model. Our data takes into account realistic pore morphology, whereas the ideal model only accounts for uniform through-thickness pores. As a result, the
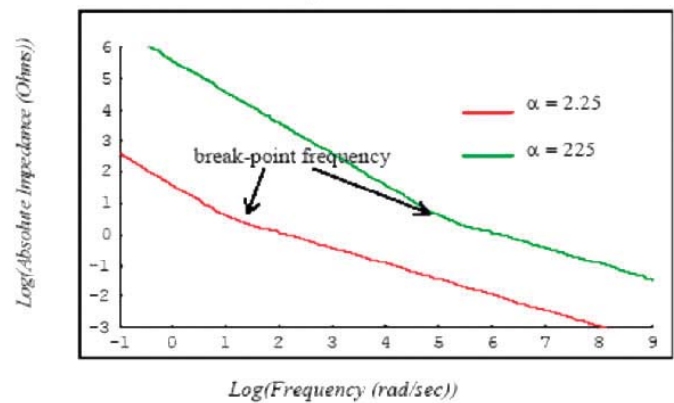
Figure 5. Model for ideal pore morphology

ideal model shows a significant decrease in the impedance at frequencies above the breakpoint frequency. Our data shows only a negligible decrease, meaning the gold acts more like a polished metal.

4. Conclusions

The results from our experiment show that as film thickness of a nanoporous metal increases, the resulting breakpoint frequency decreases. Our data agree with the ideal model in that as film thickness increases, the breakpoint frequency decreases. Yet, our data depart from the ideal model in the foreground because our data account for realistic pore morphology. As a result, the impedances at frequencies above the breakpoint frequency do not decrease as sharply as those in the ideal model.

5. Future Work

The continuation of this project is contingent upon increasing sample population of the 100 nm samples to drastically decrease the standard deviation of the breakpoint frequency. We also suggest that additional film thicknesses and the effect of varying pore size distribution on the electrochemical impedance be investigated. Lastly, we suggest that the impedance be tested with an electrolyte similar to body fluids, e.g. a Riggers solution.

Acknowledgements

References

1. Pugh, D. V., Ph.D. thesis, Virginia Polytechnic Institute and State University, Blacksburg, VA 2003.

2. Ratner, B. D.; Hoffman, A. S.; Schoen, F. J.; Lemons, J. E., eds. *Biomaterials Science: An Introduction to Materials in Medicine*. Academic Press: 1996.

3. Dursun, A., Ph.D. thesis, Virginia Polytechnic Institute and State University, Blacksburg, VA 2003.

4. Ding, Y.; Kim, Y-J.; Erlebacher, J., Nanoporous Gold Leaf – "Ancient Technology"/Advanced Material. *Advanced Materials* **2004**, 16 (21), 1897-1900.

5. Erlebacher, J.; Aziz, M. J.; Karma, A.; Dimitrov, N.; Sieradzki, K., Evolution of Nanoporosity in Dealloying. *Nature* **2001**, 410, 450-453.

6. Erlebacher, J., An Atomistic Description of Dealloying: Porosity Evolution, the Critical Potential, and Rate-Limiting Behavior. *Journal of the Electrochemical Society* **2004**, 151, C614-C626.

7. Stratmann, M.; Rohwerder, M., A Pore View of Corrosion. *Nature* **2001**, 410, 420-423.

Deposition and Single-Step Processing of YBCO Thick Films for Multilayered Electronics

Jonathan C. Langman, Matthew E. Lynch

Virginia Polytechnic Institute and State University
Department of Materials Science and Engineering
213 Holden Hall, Virginia Tech
Blacksburg, VA 24061

Abstract

The goal of this project was to successfully cofire a screen-printed yttrium barium copper oxide (YBCO) superconductor onto a low-temperature cofired ceramic (LTCC) substrate. The purpose was to investigate the compatibility of thick-film, high-temperature superconductors with multilayered ceramic (MLC) packages for cryogenic applications. Paste consisting of standard organics and YBCO powder of -325 mesh particle size was screen-printed onto Dupont 951 Green Tape. The system was cofired at temperatures ranging from 925°C to 975°C. The quality of the cofired system was characterized in several ways: Meissner diamagnetism, scanning electron microscopy, x-ray diffraction, and AC susceptibility tests were performed to determine the superconducting capability of the system. Samples cofired at 950°C retained some superconductivity after firing and showed the best compromise between sintering and degradation.

1. Introduction

Many of today's electronics depend on multilayered ceramic (MLC) packaging technology.[1] This technology allows a circuit to be constructed in three dimensions and consists of a process in which metallic conductor film is screen-printed onto a ceramic substrate, the printed substrates are stacked one on top of another, and the system is cofired.[2] An electronic package suitable for a variety of applications is the result.

Two important types of MLC substrates are high-temperature cofired ceramics (HTCC) and low-temperature cofired ceramics (LTCC).[1] The former and more outdated substrate uses a ceramic fired at high temperatures with a low-conductivity refractory metal as a conductor. The latter was developed because high-conductivity metals cannot be fired to temperatures required for sintering HTCC substrates. Important properties of LTCC substrates include low dielectric loss and the capability of being cofired with high-conductivity conductors.[1]

High-temperature superconductors (HTS), such as yttrium barium copper oxide (YBCO), are being incorporated into microwave/RF devices because of their low resistivity.[2] Thick-film YBCO is not used as a standard conductor with LTCC substrates, but the incorporation of YBCO with LTCC-based MLC packages constitutes an interesting approach to making MLC devices.

Ceramic high-temperature superconductors, though nonmetallic, meet a key requirement for MLC conductors: excellent electrical conductivity. This project inves-

tigated HTS materials as printed conductors in order to improve the conductivity of circuitry in MLC packages.

The technology of cofired MLC packages is based on the ability to cofire the conductor and the substrate without harming their respective properties. Therefore, the first step in this investigation was to demonstrate that YBCO could be cofired with a suitable, low-loss LTCC substrate.

The following is a list of objectives for the investigation:

- Deposit superconductor thick film onto unfired dielectric tape
- Evaluate the effects of conventional processing on substrate/HTS system
- Characterize the samples
- Optimize the processing parameters

2. Experimental Procedure

A screen-printable paste was developed using $YBa_2Cu_3O_{7-x}$ (YBCO) powder, a common superconductor compound, and standard organics. The YBCO powder (-325 mesh) was manufactured by SCI Engineered Materials. The organics were acetone, Heraeus RV-912 thinner, Heraeus RV-914 binder, and Sigma-Aldrich Menhadden fish oil. A silk screen and hand-squeegee were used to print a 1 in x 1 in square pattern of the paste onto the substrate.

The LTCC tape used for this experiment was DuPont 951 Green Tape with a 10 mil thickness. To increase thickness, a Dake press was used to laminate unfired tapes together.

A Thermolyne 1400 tabletop box furnace with manual temperature control was used for the cofiring operation. Due to the oxygen-sensitive nature of YBCO, the furnace was equipped with an oxygen lance that entered the furnace through a small opening in the door.

The samples were comprised of four layers of YBCO printed onto a substrate consisting of three laminated tapes. A drying step was included between printing each YBCO layer. Experimentation consisted of an evaluation of the effect of different cofiring times and temperatures on the system. Figure 1 shows the firing profile.

Combinations of three peak times (5, 10, and 15 min.) and temperatures (925°C, 950°C, and 975°C)

were used, giving a total of nine different combinations. Two samples were fired at each time/temperature combination. Processing times were controlled as closely as possible, but since a manual furnace was used, some variations of time from the nominal values occurred.
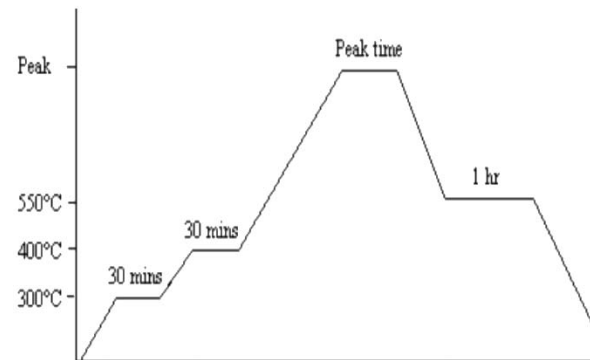
Figure 1. Firing profile for time/temperature investigation

3. Results and Discussion

3.1 Meissner Effect and Adhesion

Qualitative Meissner analysis was performed on all the samples cofired according to the above schedule. The testing consisted of scraping off particles from the film surface into a dish of liquid nitrogen and observing if the particles were repelled when introduced to a magnetic field (the Meissner effect). Table 1 shows the results. A "Yes" indicates the presence of the Meissner effect.

All samples fired at 925°C exhibited the Meissner effect, indicating that they were superconducting. Only the two samples held at 950°C for shorter times were superconducting. None of those fired at 975°C exhibited this effect. The sample fired at 975°C for 15 minutes yielded no powder for analysis because it was very hard and well-bonded to the substrate. From this qualitative analysis, it appeared that the lower time/temperature combinations provided the best results for superconductivity.

Temperature also appeared to be proportional to hardness and adhesion of the film. At 925°C, powder was readily removed when scraped for Meissner testing. In contrast, it was very difficult to get any part of any film fired at 975°C to separate from the tape. This resistance to scratching was attributed to better sintering at higher temperatures. Unfortunately, higher temperatures, while providing good bonding

Table 1. Results of Meissner test

Temperature(°C)	Time (min)		
	5	10	15
925	Yes	Yes	Yes
950	Yes	Yes	No
975	No	No	-

in the film, had a negative effect on the superconducting properties, as discussed.

A theory was devised relating the opposite effects on adhesion and diamagnetism to the four layers of YBCO paste that were deposited. At lower temperatures, the first couple of layers acted as a barrier to the glassy phase coming through from the substrate, leaving a poorly bonded pure-phase YBCO layer on top. At higher temperatures, sintering was driven at much faster rates and the glassy phase from the substrate was able to creep up and contaminate all four YBCO layers. Further research into this theory was carried out with scanning electron microscopy.

3.2 Microscopy

Microscopy was performed using a Jeol scanning electron microscope. The use of SEM provided a number of interesting details about the structure. In Figure 2, the microstructural evolution for samples held at peak temperature for 10 minutes is shown.

In Figure 2a, unsintered YBCO particles on the order of 1mm diameter are shown. Figure 2b reveals that these particles formed necks by 925°C. Figure 2c shows substantial coarsening of YBCO particles at 950°C. Finally, Figure 2d reveals very large grains at 975°C.

The microstructure of samples fired at 925°C was fairly uniform. Some cracks were visible under 2000x magnification, leaving islands of isolated material with approximate diameter of 500 nm. These cracks had a width of approximately 1μm. At 950°C, the islands were still present; however, the crack width was much smaller and barely visible at 2000x magnification. At 975°C, no cracks were visible.

As shown in Figure 2d, samples fired at 975°C contained very large grains, but some of these large regions appeared to be glassy. As time and tempera-
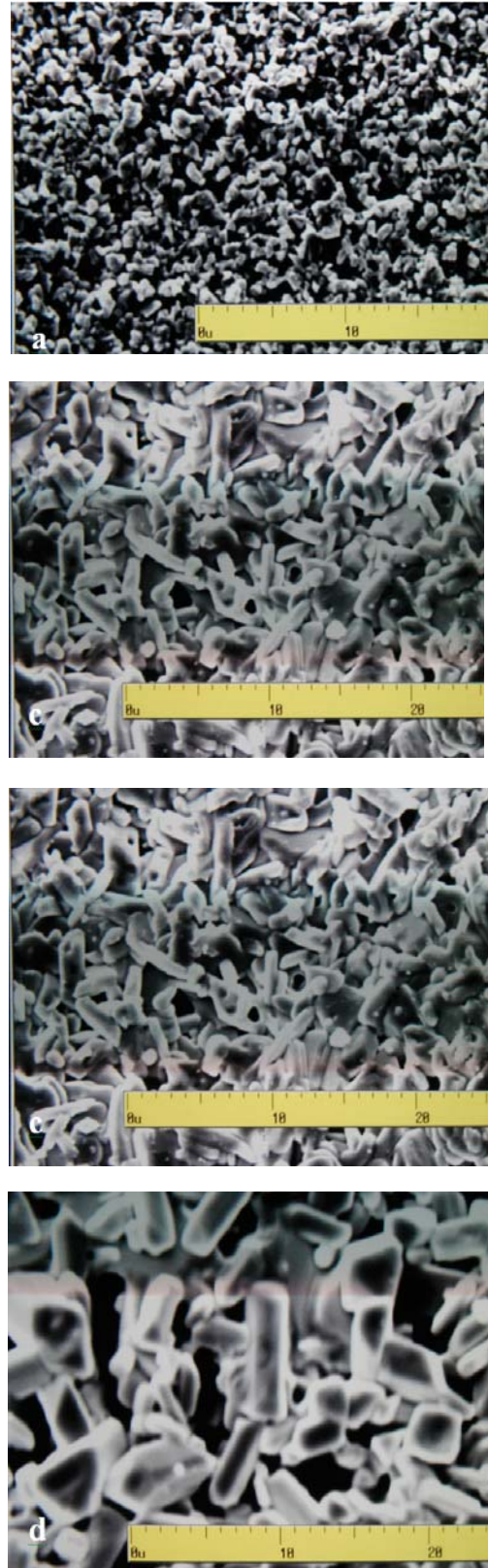

Figure 2. Difference in microstructure at various temperatures. The scale is in microns. (a) Unfired YBCO layer. (b) 925°C, 10 min. (c) 950°C, 10 min. (d) 975°C, 10 min.

ture were increased, these regions grew and became more abundant within the microstructure.

The dielectric tape contained alumina and glass frit, the latter of which was used to lower the sintering temperature. Films cofired on this substrate at 975°C had a glassy appearance and did not easily yield particles from scraping for the Meissner test. This effect was attributed to the glass frit interacting with the YBCO particles, as shown above. The same glassy phase was not observed in the YBCO samples fired at 925°C.

3.3 X-ray Analysis

X-ray powder diffraction was performed on the surface of YBCO films using a Scintag XDS 2000 diffractometer. Figure 3 shows the diffraction peaks for various samples. These peaks change with time and temperature, indicating crystallographic evolution of the film.

The sample held at 925°C for 5 minutes (Figure 3b) produced a diffraction pattern closely resembling that of phase-pure YBCO powder (Figure 3a). The diffraction pattern of the sample fired at 950°C for 10 minutes (Figure 3c) has the peak characteristics of YBCO, but peaks from another phase are visible in the region of 42-46°. The diffraction pattern of the sample fired at 975°C for 15 minutes (Figure 3d) is very cluttered and presents many non-YBCO peaks.

The diffraction data suggest that increasing time and temperature caused degradation of the YBCO film. This result was in agreement with the Meissner test and microscopy, which suggested that the lack of the Meissner effect correlated with the presence of a non-YBCO glassy phase at higher times and temperatures.

3.4 AC Susceptibility

The AC susceptibility measurements were performed on samples fired for five minutes at each temperature. Figure 4 shows the variation of m´, the real part of susceptibility, with temperature at a frequency of 100 Hz.

The superconducting transition occurs when m´ deviates from zero, indicating the expulsion of magnetic flux from superconducting regions.[3] Figure 4 shows that the transition temperature of the samples fired at 925°C and 950°C was approximately 92K, the value expected for pure YBCO, and the transition of the sample fired at 975°C was approximately 86K.
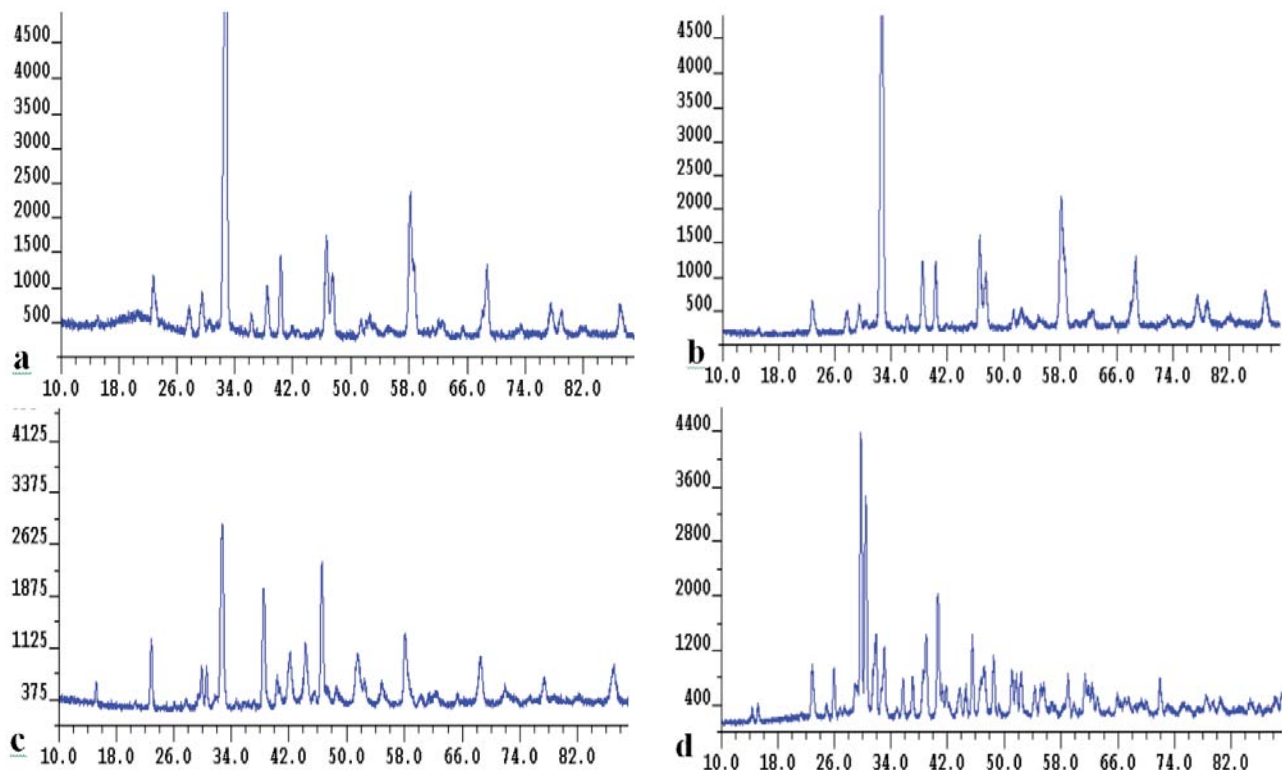
Figure 3. Diffraction patterns for (a) Pure YBCO and samples fired at (b) 925°C, 5 min. (c) 950°C, 10 min. and (d) 975°C, 15 min.

While all samples showed some degree of diamagnetism, the sample fired at 950°C had the most significant value of m´ at lower temperatures, indicating better superconducting properties. The sample fired at 975°C showed a poorer response than the other two samples.

4. Conclusions

The evidence suggests that cofiring YBCO and DuPont 951 Green Tape, while not resulting in an optimum system, is feasible. Cofiring at 950°C produced the best compromise between film sintering/adhesion and the preservation of the YBCO film properties. Firing at a higher temperature resulted in a severely degraded YBCO layer, as shown by x-ray diffraction and microscopy. This degradation translated into inferior superconducting properties, demonstrated by the Meissner test. Firing at a lower temperature produced a film that was superconducting but lacked the sintering and adhesion required for MLC packaging.
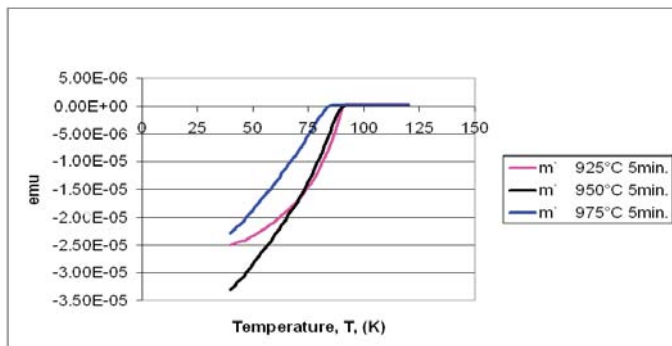
Figure 4. AC susceptibility measurements for samples fired at 5 minutes

5. Future Work

This work has demonstrated that YBCO can be cofired with a commercially available, unfired dielectric tape with some preservation of superconducting properties. An area of extension for this work includes protecting the YBCO film from degradation. Protection could be achieved by printing a buffer layer onto the tape prior to firing, thus restricting interaction between the superconductor and glass from the tape.

Acknowledgements

References

1. Wersing, W.; Dernovsek, O., Multilayer Ceramic Technology, Buchanan, R. C. (ed.), *Ceramic Materials for Electronics (3rd ed.)*, Marcel Dekker, Inc.: 2004; 581- 642.

2. Hong, J.; Lancaster, M., *Microstrip Filters for RF/Microwave Applications*, John Wiley & Sons, Inc.: 2001; 191-234.

3. Martien, D., Introduction to AC Susceptibility. http://www.qdusa.com (Retrieved 3/2005)

Biological Self-Assembled Porous Ceramics as High Temperature Insulation in Steam Transport Pipes

Seth T. Price and Elizabeth A. Marier

Virginia Polytechnic Institute and State University
Department of Materials Science and Engineering
213 Holden Hall, Virginia Tech
Blacksburg, VA 24061

Abstract

Biological self-assembled porous ceramics could serve as a substitute for asbestos in thermally insulating applications, such as steam transport pipes in coal-fired power plants. To become a viable alternative to asbestos, a biologically self-assembling ceramic would have good thermal stability up to 650°C, have low thermal conductivity, and be nontoxic and light weight. Ball clay was chosen as the base for the ceramic. By adjusting the amounts of water, yeast, salt, and sugar in the slurry, the sample with the lowest density was found, as it would be most likely to yield the highest porosity, and thus lowest thermal conductivity.

1. Introduction

Boilers in coal-fired power plants are often located a considerable distance from steam turbines. As the steam leaves the boiler and is transported towards the turbine, it cools slightly and loses pressure, which reduces the efficiency of the turbine. Temperature has more influence than pressure in terms of efficiency.[1] To combat this, power plants have traditionally wrapped their steam transport pipes in an asbestos blanket and covered the asbestos with sheet metal.

In the event of a pipe failure (due to creep, corrosion, etc.), the power company must fund an expensive asbestos clean up because of the carcinogenic nature of asbestos.[2] Due to increased health and safety concerns, asbestos is slowly being phased out and a new insulating material is being sought.

There are many conditions that must be met to produce a full engineering solution, especially for critical applications, such as power generation. The research conducted here is only a preliminary investigation of a larger problem.

1.1 Design Criteria

The material must be non-toxic, cost effective, easy to install, and lightweight. Due to the high temperatures encountered in a power plant (as much as 600°C), the material must not thermally degrade. In addition to thermal stability, it must be a comparable material to asbestos in terms of thermal conductivity to maintain, if not improve, the efficiency of the system.

1.2 Ceramic Base

Ceramics are known for high maximum operating temperatures and low thermal conductivity. Because of these characteristics, ceramic materials could serve as an asbestos replacement.

Ball clay is a safe, cost effective material that experiences very little shrinkage when fired. It is easy to process and readily available.

Thermal conductivity is difficult to measure, and finding the efficiency of an insulating material is even more complex. One established link is between closed porosity and insulating ability. Since air is a good insulator, but subject to convection currents which cool the surface, having closed porosity forces the air to remain trapped and not aid in convection cooling. Porous ceramics are commonly used in thermal insulation applications.[3]

1.3 Biological Self-Assembled Ceramics

One form of biological self-assembled ceramic is created by adding yeast to a slurry of ceramic powder, sugar, salt and water. The reaction caused by the biological agent can be qualitatively described as:

$$\text{Yeast} + \text{Sugar} \rightarrow \text{Alcohol} + CO_2 \qquad (1)$$

The yeast feeds on the sugar and generates alcohol and CO_2 bubbles. To speed up this reaction, salt is added as a catalyst.

An example of a biological self-assembled ceramic is shown in Figure 1. This material was made using kaolin to test the method.

2. Experimental Procedure

To study the feasibility of using biologically generated porous ceramics, the composition with the most beneficial physical properties was examined.

2.1 Developing a Composition

The composition given by the project advisors was a mixture of ball clay, water, sugar, salt, and yeast content. The individual constituents of this initial composition were varied to determine which components had the greatest influence on the density. Table 1 shows the initial composition in terms of a weight fraction and the weight of each constituent per typical sample.

Batches of the initial composition were used to make six samples. The large batch size allowed the material to be homogenized with an electric mixer. Once fully mixed, the batch was divided into six samples. After dividing the samples, a predetermined

Figure 1. Biologically self-assembled kaolin

amount of one of the ingredients from the batch recipe (e.g. salt, water, etc.) was added to each sample to monitor the individual influence of each ingredient on the material. One sample from each batch was unmodified as a control sample. Once poured, the samples were placed under a fume hood at 21°C and allowed to dry.

2.2 Bulk Density

The bulk density is of great importance to this study because it yields the density of the sample excluding open pores. In an insulating application, large open pores are treated as surfaces through which convection can act to transmit heat away from the pipe. Small open pores or closed pores are necessary for an insulating material.

Table 1. Initial composition

Ingredient	Weight Fraction	Weight(g)
Ball Clay	0.475	180
Water	0.359	136
Sugar	0.140	53
Salt	0.00132	3
Yeast	0.00312	7.1

A representative piece of each fired sample was tested for density. The density equation and method are shown in Equation 2 where ρ_s was the density of the ceramic, ρ_w was the density of the water in the container, w_w was the mass of a container filled only with water, w_{cs} was the mass of the sample submersed in water at in the container, and w_s was the mass of the sample.

$$r_s = \frac{\left(\dfrac{w_w - (w_{cs} - w_s)}{r_w}\right)}{w_s} \qquad (2)$$

2.3 Temperature Stability

Temperature stability of the samples was evaluated qualitatively by placing a piece of each of the samples in a box furnace at 650°C for 12 hours in air to note any significant volume changes. It was assumed that after 12 hours, the organic material was completely burned out, and further shrinkage would not occur.

3. Results and Discussion

The amounts of each constituent were varied and summarized in Table 2.

3.1 Control Samples

The control samples from each batch were comparable in consistency and appearance, indicating that the test conditions from batch to batch were similar. This is an important conclusion, since some batches were manufactured on different dates, and an error in a batch would have appeared in the control sample for that batch as well.

3.2 Varying Water Content

Although reaction time was not measured, it varied significantly with water content. Additional water led to faster reaction times and faster drying times. Some of each of the samples with additional water was lost, as the reaction caused the material to overflow the sample containers.

The samples with additional water also produced the samples with the largest pores. Large closed pores are only slightly better than open pores, in that a large pore can contain a substantial convection current.

Table 2. Compositions of samples A-R

Sample	Water (g)	Sugar	Salt (g)	Yeast (g)	PVA (g)
A	136	67	3	7	0
B	136	78	3	7	0
C	136	103	3	7	0
D	136	53	6	7	0
E	136	53	10	7	0
F	136	53	15	7	0
G	236	53	3	7	0
H	176	53	3	7	0
I	156	53	3	7	0
J	146	53	3	7	0
K	136	53	3	7	0
L	136	53	3	7	0
M	136	53	3	14	0
N	136	53	3	21	0
O	136	53	3	28	0
P	136	53	3	7	12.4
Q	136	53	3	7	9.6
R	136	53	3	7	4.9

3.3 Varying Sugar Content

The samples created with additional sugar were very porous, but exhibited differential drying, with the bottom of the samples drying faster than the top.

3.4 Varying Salt Content

Visibly, there was no difference between the control samples and the samples with additional salt. The samples are slightly more fragile when handled than the control samples, which might indicate that excess salt created a defect in the ceramic matrix.

3.5 Varying Biological Agent Content

Yeast was varied by adding yeast packets, each packet weighing 7g. Since the initial composition contained one packet, the three additional test compositions had two, three, and four packets of yeast.

These samples had a slight brownish discoloration, which mostly collected at the bottoms of the sample containers. This could be due to excess yeast starving and sinking into the slurry.

3.6 Varying Binder Content

Poly(vinyl alcohol) (PVA) was added to three samples in hopes of capturing the reaction at its maximum volume change. PVA was chosen solely based on its availability in the laboratory.

The PVA did not mix well with the slurry. It is suspected that the PVA was not water soluble, and thus it sunk through the slurry and settled at the bottom of the sample holders in all three samples.

3.7 Thermal Stability

All samples survived a 12h, 650°C firing with very little shrinkage. Weight loss was significant, as the water evaporated and the organics were lost. This meant that the fired samples were less dense than the unfired samples.

3.8 Densities of Fired Compositions

Table 3 shows the densities of the as-fired samples. The densities did not vary in a predictable fashion. Even those of the control samples K and L varied wildely.

4. Conclusions

The use of biologically self-assembled ceramics might be feasible as steam transport pipe insulation. Since all of the samples survived thermal testing, without significant warping or cracking, they all were eligible for further testing.

Unfortunately, a correlation between any of the single ingredients and the amount of closed porosity could not be drawn. Because of this, further research should be conducted using the initial composition.

5. Future Work

This report is just the initial research on the feasibility of using a biologically self-assembled porous ceramic for insulation material.

5.1 Bonding and Firing

Bonding and firing test should be conducted on the sample of the most ideal composition. This test will involve dipping several small plates of Inconel 740 (a commonly used steam pipe alloy) into a slurry of the ideal composition. The plate will then be fired in a box furnace in air. This test will determine whether there is any corrosion of the Inconel plate by the material.

Another concern is a partial bonding scenario where the plate partially bonds to the material, but then differences in thermal expansion cause the material to crack

Table 3. Densities of fired compositions

Sample	Density (g/cm^3)
A	6.1 ± 0.05
B	2.6 ± 0.05
C	3.3 ± 0.05
D	4.5 ± 0.05
E	1.6 ± 0.05
F	2.2 ± 0.05
G	3.1 ± 0.05
H	2.2 ± 0.05
I	1.2 ± 0.05
J	2.1 ± 0.05
K	2.3 ± 0.05
L	1.2 ± 0.05
M	1.1 ± 0.05
N	1.4 ± 0.05
O	5.1 ± 0.05
P	3.8 ± 0.05
Q	0.2 ± 0.05
R	1.5 ± 0.05

5.2 Thermal Expansion

Due to the drastic temperature changes in steam pipes, thermal expansion data should be collected before attempting to use any material for insulation. Thermal expansion can be measured with a dilatometer, insuring that there are no unexpected phase changes during heating and cooling.

5.3 Varying Drying Temperature

The time required for the mixture to dry and harden is dependent on the drying temperature. All data collected thus far have been on samples dried in a fume hood at room temperature (21°C). A higher

drying temperature will begin to kill the biological agent; therefore, there is a peak temperature above which yeast begins to die and below which the yeast does not react as quickly.

In the power plant, finding the peak temperature response of the insulation is important to evaluate the feasibility of simply "turning on the power" to dry, harden and fire the porous ceramic.

5.4 Varying Sugar and Biological Agent Content

Since the sugar and yeast are dependent on each other, further testing should include varying sugar and yeast together. It is possible that additional yeast in tests starved, rather than reacting to its full potential.

5.5 Varying Binder

Though the samples in this experiment showed little effect due to an added binder, further research could be directed at trying other binders in different amounts. A proper composition with a binder at the proper drying rate could capture the ceramic at its maximum volume, and thus minimum density.

Acknowledgements

References

1. Swanekampe, R., Return of the Supercritical Boiler. *Power* **2002**, 146 (4), 32-40.

2. Lefton, S.A.; Besuner, P.M.; Grimsrud, G.P., The Real Cost of Cycling Powerplants: What You Don't Know Will Hurt You. *Power* **2002**, 146 (8), 29-34.

3. Sousa, E.; Silveira, C.B.; Fey, T.; Greil, P.; Hotza, D.; Novaes de Oliveira, A.P., LZSA Glass Ceramic Foams Prepared by Replication Process. *Advances in Applied Ceramics* **2005**, 104 (1), 22-29.

Virginia Tech MSE Faculty & Staff

Professors

Alex O. Aning
Associate Professor

Ph.D.,1982, University of Missouri-Rolla
Materials Processing, Mechanical Alloying,
Noncrystalline and Nanocrystalline Alloys
aaning@vt.edu (540) 231-6849

Levon V. Asryan
Associate Professor

Ph.D., 1988, Ioffe Institute of Physics and
Technology, St. Petersburg, Russia
Semiconductors, Optoelectronics,
Nanophotonics, Quantum Dot Lasers
asryan@mse.vt.edu (540) 231-7033

Jesse J. Brown Jr.
Professor Emeritus

Ph.D., 1964, Pennsylvania State University
Ceramics, Refractories, Phase Equilibria
jjbrown@vt.edu (540) 231-6777

David E. Clark, PE
Professor and Department Head

Ph.D., 1976, University of Florida
Ceramics, Microwaves, Sol-Gel, Glass
Corrosion, Ceramic Superconductors
dclark@vt.edu (540) 231-6640

Richard O. Claus
Lewis A. Hester Professor, MSE & ECE

Ph.D., 1977, Johns Hopkins University
Fiber Optics, Optical Materials and
Applications
roclaus@vt.edu (540) 231-7203

Sean G. Corcoran
Associate Professor

Ph.D., 1994, Johns Hopkins University
Corrosion, Electrochemical Modification of
Materials, Nanoporous Metals
sgc@vt.edu (540) 357-0188

Norman E. Dowling, PE
Professor, MSE & ESM

Ph.D., 1972, University of Illinois,
Urbana-Champaign
Mechanical Behavior of Materials, Fatigue,
Fracture
ndowling@vt.edu (540) 231-5399

Diana Farkas
Professor

Ph.D., 1980, University of Delaware
Simulation, Intermetallic Alloys, Defect
Structures, Interfaces, Diffusion
diana@vt.edu (540) 231-4742

Gerald V. Gibbs
University Distinguished Professor Emeritus

Ph.D., 1962, Pennsylvania State University
Mathematical Crystallography, Computer
Modeling
gvgibbs@vt.edu (540) 231-6330

Louis J. Guido
Associate Professor, MSE & ECE

Ph.D., 1989, University of Illinois,
Urbana-Champaign
Semiconductor Alloys, Quantum
Structures, Electronic and Photonic Devices
louis.guido@vt.edu (540) 231-3551

D. P. H. Hasselman
Professor Emeritus

Ph.D., 1966, University of California,
Berkeley
Mechanical and Thermal Properties, Stress
Fracture
hasselmn@vt.edu (540) 231-2284

Stephen L. Kampe
Professor

Ph.D., 1987, Michigan Technological
University
Materials Processing, Composites, Mechanical
Behavior
kampe@vt.edu (540) 231-8688

Kathryn V. Logan, PE
Virginia Tech Langley Professor

Ph.D., 1992, Georgia Institute of Technology
Multi-functional Materials, Design of
Materials
klogan@mse.vt.edu (540) 231-2080

William T. Reynolds, Jr.
Professor

Ph.D., 1988, Carnegie Mellon University
Phase Transformations, Physical Metallurgy
reynolds@vt.edu (540) 231-6825

Brian J. Love
Professor

Ph.D., 1990, Southern Methodist University
Polymeric Based Adhesives, Interfacial Sur-
face Analysis, Biomaterials, Polymer Dielec-
trics, Composites
blove@vt.edu (540) 231-3186

Dwight D. Viehland
Professor

Ph.D., 1991, Pennsylvania State University
Electrical and Dielectric Properties,
Ferroelectrics and Piezoelectrics, Phase
Transformations
viehland@mse.vt.edu (540) 231-2276

Peizhen Kathy Lu
Assistant Professor

Ph.D., 2000, Ohio State University
Nanomaterials, Graded Materials, Multifunc-
tional Materials, Material Design
klu@mse.vt.edu (540) 231-3225
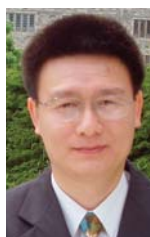
Yu Wang
Assistant Professor

Ph.D., 2001, Rutgers University
Materials Modeling, Simulation,
Microstructure Evolution, Multiferroic Materials
yuwang@mse.vt.edu (540) 231-2754

Affiliated and Adjunct Professors

Guo-Quan (GQ) Lu
Professor, MSE & ECE

Ph.D., 1990, Harvard University
Synthesis and Processing of Materials,
Reliability Evaluation, Semiconductor
Materials, Solid State Lighting Systems
gqlu@vt.edu (540) 231-8686

Romesh C. Batra, Affiliate
Clifton C. Garvin Professor, ESM

Ph.D., 1972, Johns Hopkins University
Computational Solid Mechanics, Metal
Forming, Smart Materials/Structures,
Carbon Nanotubes
rbatra@vt.edu (540) 231-6051

Marie C. Paretti
Assistant Professor, EngE
Director, MSE/ESM Advanced Engineering
Communications Program

Ph.D., 1997, University of Wisconsin-Madison
Technical Communications, Engineering Pedagogy
mparetti@vt.edu (540) 231-7520

James R. Heflin, Affiliate
Associate Professor, Phys

Ph.D., 1990, University of Pennsylvania
Organic Optoelectronic Self-Assembled
Nanostructures
rheflin@vt.edu (540) 231-4504

Gary R. Pickrell
Assistant Professor

Ph.D., 1994, Virginia Tech
Photonics, Porous Materials, Biologically
Derived Nanoscale Materials
pickrell@vt.edu (540) 231-3504

Robert W. Hendricks, Affiliate
Professor, ECE

Ph.D., 1987, Cornell University
Electronic Materials, Solid State Physics,
Semiconductor Processing
Robert.Hendricks@vt.edu (540) 231-6917

Herve Marand, Affiliate
Professor, Chem

Ph.D., 1988, University of Massachusetts
Semicrystalline Polymers, Phase Separation in
Binary Polymers, Crystallization of Polymers
in Confined Space
hmarand@vt.edu (540) 231-5391

Roe-Hoan Yoon, Affiliate
Nicolas T. Camicia Professor, MinE
Dir., Center for Advanced Separation Technologies

Ph.D., 1977, McGill University
Surface Forces, Electrochemistry, Column
Flotation, Coal Cleaning and Dewatering
ryoon@vt.edu (540) 231-7056

Maureen M. Julian, Adjunct
Assistant Professor

Ph.D., 1966, Cornell University
Crystallography, Absorption Edges, Epitaxial
Relationships
erie@vt.edu (540) 231-7123

Ronald G. Kander, Adjunct
Professor and Department Head, ISAT
James Madison University

Ph.D., 1987, University of Delaware
Rapid Prototyping and Tooling, Polymer
Processing and Characterization
kanderrg@jmu.edu (540)568-2740

Michael J. Kelley, Adjunct
Professor, APS
College of William and Mary

Ph.D., 1973, Rensselaer Polytechnic Institute
Polymer Surface Modification by UV or IR
Light, Surface Science
mikelley@vt.edu (540) 231-8688

H. Felix Wu, Adjunct
ComSci Fellow, Program Manager,
Comp. Civ. Const., CLSO, ATP, NIST

Ph.D., 1988, Cornell University
Fibers, Polymers, Composites, Structural
Monitoring, Interfaces, Lifetime Prediction
felix.wu@nist.gov (301) 975-4685

Research Faculty and Instructors

Christine B. Burgoyne
Assistant Director, MSE/ESM Engineering
Communication Program

M.A, 2001, Virginia Tech
Global and Engineering Communications,
Critical Discourse Analysis
cbala@vt.edu (540) 231-5305

Shuxiang Dong
Research Scientist

Ph.D., 1993, Tsinghua University
Piezoelectric Micromotors, Actuators, Magnetic Sensors, Gas Sensors and Acoustic
Transducers.
sdong@mse.vt.edu (540) 231-2327

LeeAnn C. Ellis
Research Associate
Public Relations Specialist

B.El.Ed., 1985, Virginia Tech
mse@vt.edu (540) 231-6777

Diane C. Folz
Senior Research Associate

B.S., 1987, University of Florida
Microwave Processing, Ceramics, Waste Remediation and Recycling, Surface Modification
dfolz@vt.edu (540) 231-3897

Joerg R. Jinschek
Research Assistant Professor, MSE & GeoS

Ph.D. (Dr.rer.nat.), 2001, Friedrich-Schiller-University Jena, Germany
High-resolution TEM, Electron Spectroscopy,
Semiconductors
jrjinschek@vt.edu (540) 231-6640

Jie-Fang Li
Research Associate Professor

Ph.D., 1992, Pennsylvania State University
Properties and Applications of
Multi-functional Materials
jiefang@vt.edu (540) 231-6928

Sean P. Mc Ginnis
Senior Research Scientist, MSE & BSE
Director, Green Engineering

Ph.D., 1995, Stanford University
Green Engineering, Sustainable Manufacturing,
Thin Film Adhesion, Biomimetic Materials
ctas@vt.edu (540) 231-7043

Catherine E. Fisher
Business Services Assistant

cfisher@mse.vt.edu
(540) 231-6640

Kathleen L. Rohr
Instructor

M.S., 1986, Virginia Tech
Materials Characterization, Failure Analysis
krohr@vt.edu (540) 552-3742

Amy G. Hill
Business Manager

amyhill@vt.edu
(540) 231-9125

Thomas W. Staley
Instructor

Ph.D., 2000, Virginia Tech
Crystallography, Modeling of Dynamical
Diffraction, Acoustics Science and
Technology Studies
tstaley@vt.edu (540) 231-6547

Tracey J. Keister
Office Manager

tkeister@vt.edu
(540) 231-9469

Carlos T.A. Suchicital
Research Associate Professor
Facilities Manager

Ph.D., 1988, University of Illinois
Rapid Prototyping, Microelectronics,
Microwaves, Ceramics
ctas@vt.edu (540) 231-7043

Susette W. Sowers
Program Support Technician and
Graduate Services Coordinator

susette@vt.edu
(540) 231-3178

Staff

David W. Berry
Senior Facilities Technician

dwberry@vt.edu
(540) 231-5873

Peter J. West
Information Tech Specialist, MSE & MinE

pjwest@vt.edu
(540) 231-5817

Jan L. Doran
Undergraduate Services Coordinator

jandoran@vt.edu
(540) 231-1768

Virginia Tech MSE Advisory Board

Catherine A. Baker

Systems Engineer
The Boeing Company

Charles Blankenship, Jr.

General Manager
Small Commercial Engine Operations
General Electric Company

Claudio A. Caprio

Technology Product Development
Advanced Digital Systems
BAE Systems

Richard P. Gangloff

Ferman W. Perry Professor and Chair
Materials Science and Engineering
University of Virginia

Paul Huffman

President
Dominion Metallurgical, Inc.

Alfred E. Knobler (Ex Officio)

Chairman & Chief Executive Officer
(retired)
Pilgrim Glass Corporation

John H. Kroehling

President
J.H. Kroehling &Associates

Edmund H. Moore

Program Manager
Air Force Research Laboratory

Arvid Pasto

Manager, EERE and Technology Programs
Director, High Temperature Materials Lab.
Metals & Ceramics Division
Oak Ridge National Laboratory

David Rice

Manager
Advanced Materials Technology
Northrop Grumman Newport News

Kathleen Richardson

Director
School of Materials Science &
Engineering
Clemson University

Mark Shuart

Associate Director
Transformation Projects
NASA Langley Research Center

Warren White, Sr.

Project Engineer
Northrop Grumman Newport News

George Wicks

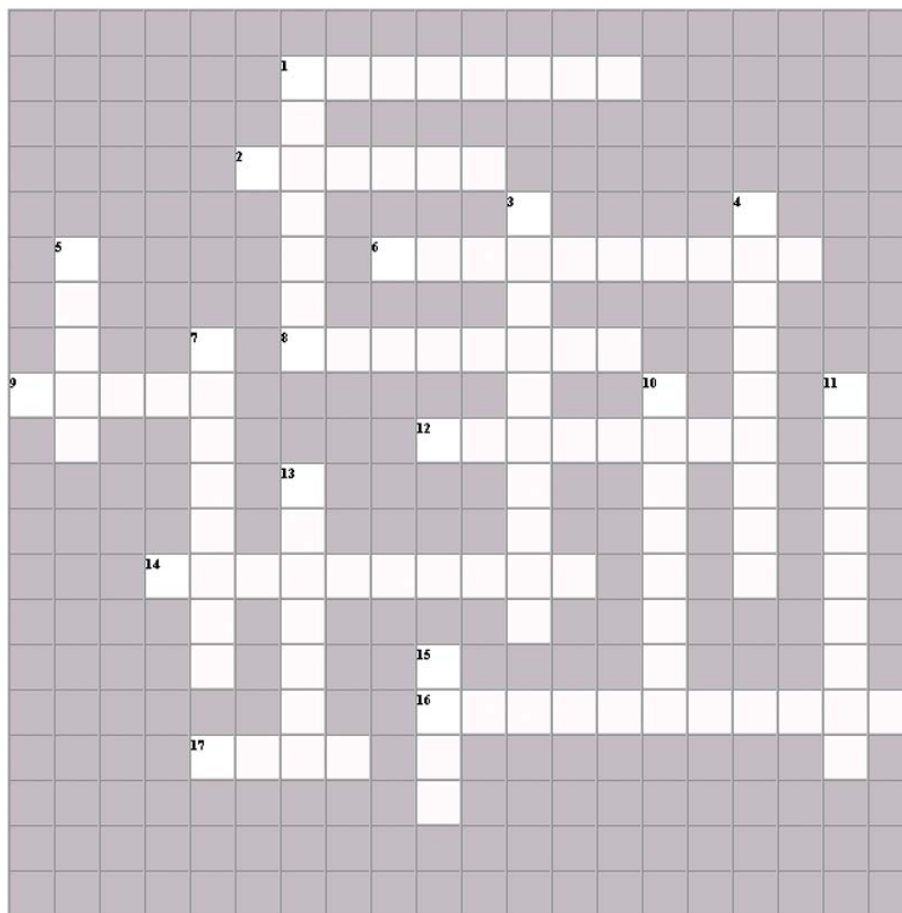Consulting Scientist
Westinghouse Savannah River
Company

Warren Wolf

President, Warren W. Wolf, Jr. Services
President, American Ceramic Society
Chief Scientist Emmeritus, Owens Corning

Crossword Challenge

answers can be found at http://www.jumr.mse.vt.edu
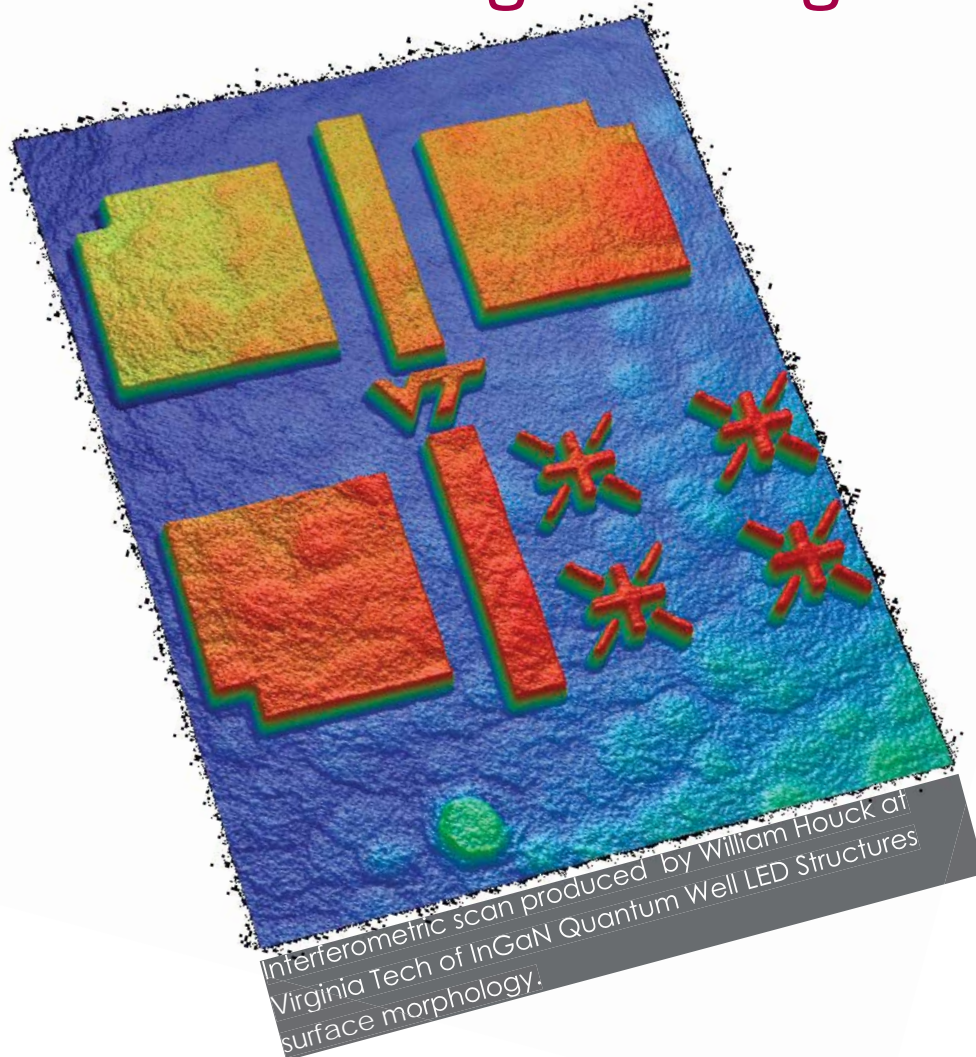
Across

1. The abstracts for the next volume of this journal are due in ___ of next year.

2. Pores were created by using a single cell ___.

6. LTC substrates have low ___ loss.

8. Fuel cells convert ___ energy to electrical energy.

9. Sand blasting to remove the top layers of glass and reveal subsequent layers is used to create ___ glass pieces.

12. Increasing the laser intensity increased the ___ of the SLS pieces.

14. In the porous polymer the size and shape of the pores will be that of the ___ agent.

16. In steam transport, ___ has more influence than pressure in terms of efficiency.

17. ___ is the acronymn for this journal.

Down

1. Electrical systems can be replaced by ___ systems utilizing freeform manufacturing.

3. Transducers convert mechanical motion to ___ energy.

4. Transduction of IPMCs are affected by ___ and ionic radii.

5. As nanoporous gold film thickness increases, ___ point frequency decreases.

7. For nanoporous gold, impedence depends on ___.

10. YBCO samples at 925ºC showed the ___ effect.

11. Ionic polymer metal composistes were investigated for ___ and sensors.

13. Alfred Knobler created the ___ Glass Company.

15. Functional limitations for SLS depend on the ___ size.

Want to be a part of creating something exciting?

Interferometric scan produced by William Houck at Virginia Tech of InGaN Quantum Well LED Structures surface morphology.

Submit your project to the Fall 2006 JUMR.

If you are an undergraduate at any institution and working on a materials research-related project, **submit a self-contained abstract**, consisting of no more than 200 words for consideration for next year's issue. It should outline the aims, scope, and conclusions of your work.

Based on these abstracts, authors will be selected to provide a 2-5 page manuscript to be reviewed for publication. Please submit abstracts by **February 17, 2006.** Abstracts and questions should be submitted to:

JUMR
213 Holden Hall
Virginia Tech
Blacksburg, VA 24061
or
jumr@mse.vt.edu
http://www.jumr.mse.vt.edu

2005 MRS FALL MEETING

www.mrs.org/meetings/fall2005/

SYMPOSIA

ENERGY AND THE ENVIRONMENT

A: The Hydrogen Cycle—Generation, Storage, and Fuel Cells
B: Next-Generation Batteries, Supercapacitors and Other Storage Materials
C: Material Innovations for High-Performance Building Systems
D: Organic and Nanostructured Composite Photovoltaics and Solid-State Lighting
E: Electrochromic Materials and Applications
F: Materials and Technologies for Direct Thermal-to-Electric Energy Conversion
G: Life-Cycle Analysis Tools for "Green" Materials and Process Selection
H: Multifunctional Energetic Materials

BIO-ORGANIC/INORGANIC COMPOSITES

I: Interfaces in Organic and Molecular Electronics II
J: Biomimetic Polymers and Gels
K: Engineering Biointerfaces via Cell-Interactive Materials
L: Mechanical Behavior of Biological and Biomimetic Materials
M: Flexible and Printed Electronics, Photonics, and Biomaterials

NANO- TO MICROSTRUCTURED MATERIALS

N: Dynamics in Small Confining Systems VIII
O: Nanoparticles and Nanostructures in Sensors and Catalysis
P: Quantum Confined Semiconductor Nanostructures— Fabrication, Physical Properties, and Applications
Q: Degradation Processes in Nanostructured Materials
R: Assembly at the Nanoscale—Toward Functional Nanostructured Materials
S: Nanomaterials and the Environment

SMART MATERIALS AND DEVICES

T: Ferroelectric Thin Films XIV
U: Multiferroic Materials
V: Materials and Devices for Smart Systems
W: Electroresponsive Polymers and Their Applications

MECHANICAL BEHAVIOR

Y: Surface Interactions and Surface Engineering for Manufacturing Applications
Z: Amorphous and Nanocrystalline Metals for Structural Applications
AA: Micro- and Nanomechanics of Structural Materials
BB: Mechanisms of Mechanical Deformation in Brittle Materials

ELECTRONICS AND PHOTONICS

CC: Photophysical Properties of Monolayers on Nanomaterials and Surfaces
DD: Materials for Transparent Electronics
EE: Progress in Semiconductor Materials V—Novel Materials and Electronic and Optoelectronic Applications
FF: GaN, AlN, InN, and Related Materials

GG: Plasmonics—Nanoscale Optics and Photonics Based on Metals
HH: Magnetic Sensors and Sensing Systems
II: Fabrication and Characterization Methods for Novel Magnetic Nanostructures

GENERAL INTEREST

X: Frontiers of Materials Research
JJ: Actinides—Basic Science, Applications, and Technology
KK: Solid-Solid Interfaces from Observation to Modeling
LL: Combinatorial Methods and Informatics in Materials Science
MM: *In-Situ* Electron Microscopy of Materials
NN: Scanning Probe Microscopy in Materials Research
OO: Growth, Modification, and Analysis by Ion Beams at the Nanoscale

SPECIAL FORUMS

PP: Forum on Materials Science Education
QQ: IP, TT, VC, IPO, and U

MEETING ACTIVITIES

SYMPOSIUM TUTORIAL PROGRAM

Available only to meeting registrants, the symposium tutorials will concentrate on new, rapidly breaking areas of research.

EXHIBIT AND RESEARCH TOOLS SEMINARS

A major exhibit encompassing the full spectrum of equipment, instrumentation, products, software, publications, and services is scheduled for November 29−December 1 in the Hynes Convention Center, convenient to the technical session rooms. Research Tools Seminars, an educational seminar series that focuses on the scientific basis and practical application of commercially available, state-of-the-art tools. will be held again this fall.

PUBLICATIONS DESK

A full display of over 860 books, plus videotapes and electronic databases, will be available at the MRS Publications Desk.

SYMPOSIUM ASSISTANT OPPORTUNITIES

Graduate students planning to attend the 2005 MRS Fall Meeting are encouraged to apply for a Symposium Assistant position and/or a Graduate Student Award.

CAREER CENTER

A Career Center for MRS members and meeting attendees will be open Tuesday through Thursday.

Meeting Chairs:

Yang-Tse Cheng
General Motors R&D Center
Tel 586-986-0939
Fax 586-986-3091
yang.t.cheng@gm.com

David S. Ginley
National Renewable Energy Laboratory
Tel 303-384-6573
Fax 303-384-6430
david_ginley@nrel.gov

Kathryn E. Uhrich
Rutgers University
Tel 732-445-0361
Fax 732-445-7036
uhrich@rutchem.rutgers.edu

Ralf B. Wehrspohn
Paderborn University
Tel 49-5251-60-2748
Fax 49-5251-60-3247
wehrspohn@physik.uni-paderborn.de

For additional meeting information, visit the MRS Web site at

www.mrs.org/meetings/

or contact:

MRS

Member Services
Materials Research Society

506 Keystone Drive
Warrendale, PA 15086-7573
Tel 724-779-3003
Fax 724-779-8313
E-mail: info@mrs.org

The 2005 MRS Fall Meeting will serve as a key forum for discussion of interdisciplinary leading-edge materials research from around the world. Various meeting formats—oral, poster, round-table, forum and workshop sessions—are offered to maximize participation.

Virginia Tech

1872